Biomedicine & Pharmacotherapy 144 (2021) 112330

Contents lists available at ScienceDirect

Biomedicine & Pharmacotherapy

journal homepage: www.elsevier.com/locate/biopha

# JKST6, a novel multikinase modulator of the BCR-ABL1/STAT5 signaling pathway that potentiates direct BCR-ABL1 inhibition and overcomes imatinib resistance in chronic myelogenous leukemia

Haidée Aranda-Tavío [a], Carlota Recio [a], Pedro Martín-Acosta [b], Miguel Guerra-Rodríguez [a], Yeray Brito-Casillas [a], Rosa Blanco [c], Vanessa Junco [c], Javier León [c], Juan Carlos Montero [d], Lucía Gandullo-Sánchez [d], Grant McNaughton-Smith [f], Juan Manuel Zapata [e], Atanasio Pandiella [d], Angel Amesty [b], Ana Estévez-Braun [b], Leandro Fernández-Pérez [a,*], Borja Guerra [a,*]

[a] Instituto Universitario de Investigaciones Biomédicas y Sanitarias (IUIBS), Farmacología Molecular y Traslacional (BIOPharm), Universidad de Las Palmas de Gran Canaria (ULPGC), Las Palmas de Gran Canaria, Spain
[b] Instituto Universitario de Bio-Orgánica "Antonio González" (IUBO), Departamento de Química Orgánica, QUIBIONAT, Universidad de La Laguna (ULL), La Laguna, Spain
[c] Instituto de Biomedicina y Biotecnología de Cantabria (IBBTEC), Universidad de Cantabria-CSIC, Santander, Spain
[d] Instituto de Biología Molecular y Celular del Cáncer, CSIC and CIBERONC. Institute of Biomedical Research of Salamanca (IBSAL), Salamanca, Spain
[e] Instituto de Investigaciones Biomédicas "Alberto Sols" - CSIC, Universidad Autónoma de Madrid, Madrid, Spain
[f] Centro Atlántico del Medicamento (CEAMED) SA, La Laguna, Tenerife, Spain

ARTICLE INFO

*Keywords:*
Chronic myelogenous leukemia
BCR-ABL1
Synergism
Imatinib resistance

ABSTRACT

Chronic myelogenous leukemia (CML) is a hematological malignancy that highly depends on the BCR-ABL1/STAT5 signaling pathway for cell survival. First-line treatments for CML consist of tyrosine kinase inhibitors that efficiently target BCR-ABL1 activity. However, drug resistance and intolerance are still therapeutic limitations in Ph+ cells. Therefore, the development of new anti-CML drugs that exhibit alternative mechanisms to overcome these limitations is a desirable goal. In this work, the antitumoral activity of JKST6, a naphthoquinone-pyrone hybrid, was assessed in imatinib-sensitive and imatinib-resistant human CML cells. Live-cell imaging analysis revealed JKST6 potent antiproliferative activity in 2D and 3D CML cultures. JKST6 provoked cell increase in the subG1 phase along with a reduction in the G0/G1 phase and altered the expression of key proteins involved in the control of mitosis and DNA damage. Rapid increases in Annexin V staining and activation/cleavage of caspases 8, 9 and 3 were observed after JKST6 treatment in CML cells. Of interest, JKST6 inhibited BCR-ABL1/STAT5 signaling through oncokinase downregulation that was preceded by rapid polyubiquitination. In addition, JKST6 caused a transient increase in JNK and AKT phosphorylation, whereas the phosphorylation of P38-MAPK and Src was reduced. Combinatory treatment unveiled synergistic effects between imatinib and JKST6. Notably, JKST6 maintained its antitumor efficacy in BCR-ABL1-T315I-positive cells and CML cells that overexpress BCR-ABL and even restored imatinib efficacy after a short exposure time. These findings, together with the observed low toxicity of JKST6, reveal a novel multikinase modulator that might overcome the limitations of BCR-ABL1 inhibitors in CML therapy.

## 1. Introduction

Chronic myelogenous leukemia (CML) is a hematopoietic stem cell disease associated with abnormal proliferation of clonal cells of the myelogenous lineage [1]. This malignant myeloproliferative disorder is characterized by a chromosomal translocation t(9;22)(q34;q11) that provokes Philadelphia (Ph) chromosome emergence, a hallmark present in 95% of CML cases but also at lower frequencies in acute lymphoblastic

* Corresponding authors at: Instituto Universitario de Investigaciones Biomédicas y Sanitarias (IUIBS), Farmacología Molecular y Traslacional (BIOPharm), Universidad de Las Palmas de Gran Canaria (ULPGC), Las Palmas de Gran Canaria, Spain.
*E-mail addresses:* leandrofco.fernandez@ulpgc.es (L. Fernández-Pérez), borja.guerra@ulpgc.es (B. Guerra).

https://doi.org/10.1016/j.biopha.2021.112330
Received 3 September 2021; Received in revised form 6 October 2021; Accepted 8 October 2021
Available online 19 October 2021

leukemia (ALL) and acute myeloid leukemia (AML) [2]. The resulting fused genes of the Ph chromosome encode the BCR-ABL1 oncogenic protein, whose constitutively active tyrosine kinase represents the keystone of CML pathogenesis [3]. BCR-ABL1 activates different intracellular signaling pathways, including RAS/RAF/MAPK, PI3K/AKT and JAK/STAT, which are involved in the control of cell survival and proliferation, among other key cellular responses [4]. Dysregulation of JAK/STAT signaling is indeed a common factor in hematological cancers, particularly in CML, where BCR-ABL1 can directly and indirectly activate STAT5, resulting in the overexpression of proto-oncogenic target genes (e.g., *MYC* and *PIM1*) [4,5]. Thus, BCR-ABL1/STAT5 signaling triggers enhanced proliferation of CML clones and genomic instability, sustaining the conditions for a tumoral environment [6,7]. Given the above findings, it is not surprising that targeting BCR-ABL1 has marked a milestone in the treatment of CML.

In 2001, the Food and Drug Administration (FDA) approved the first tyrosine kinase inhibitor (TKI), imatinib mesylate (IM), which binds the BCR-ABL1 catalytic domain, blocking its activation [8]. Twenty years later, a broader spectrum of TKIs is available as first-line treatment for CML [9], allowing most early diagnosed CML patients to reach a near-normal life expectancy. However, TKIs exhibit key limitations in CML therapy, including some serious side effects mainly associated with second-generation TKIs, the emergence of TKI resistance, and the requirement for long-term medication, which triggers high economic costs [9,10]. Approximately 30–50% of CML patients discontinue IM therapy after 5 years, mainly due to the emergence of treatment resistance (15–20%) and intolerance (5–7%) [11]. Hence, mechanisms involved in the generation of IM resistance have been extensively investigated. Interestingly, some are defined as BCR-ABL1-dependent mechanisms (e.g., augmented expression of the *BCR-ABL1* gene or mutations affecting the kinase domain of BCR-ABL1 that dodge TKI binding, such as T315I) [12], whereas others are categorized as BCR-ABL1-independent processes (e.g., alterations of efflux influx pumps, quiescent CML stem cell persistence, additional chromosomal abnormalities emergence or SRC family tyrosine kinases overexpression) [8,12,13].

Regarding BCR-ABL1-dependent TKI resistance, it has been demonstrated that the expression levels of the oncoprotein are unaltered with the inhibition of its kinase activity. Consequently, CML patients receiving TKI therapy normally need continuous treatment. Moreover, BCR-ABL1 can act as a scaffold protein, establishing signaling networks that are modified but not blocked by TKIs [14,15]. For these reasons, compounds able to reduce not only kinase activity but also the levels of the oncoprotein itself may represent an effective alternative therapy for CML. Importantly, the potential relevance of this alternative pharmacological strategy has recently been reinforced by the advent of PROTACs (proteolysis targeting chimeras), which employ the ubiquitin-mediated degradation system to target oncogenic proteins [16], or the use of CRISPR (clustered regularly interspaced short palindromic repeats) technology to provide permanent oncogene knockout [17] in CML models.

BCR-ABL1-independent IM resistance is associated with increased alternative survival signaling pathways (e.g., RAF/MEK/ERK) that confer apoptosis protection [18]. In this sense, preclinical and clinical studies have suggested that the combination of TKIs with multikinase inhibitors might be an attractive alternative to selective TKIs alone. Considering all these insights, identifying alternative drugs that overcome the main limitations of current CML treatments is an important goal to be achieved by the cancer research community.

Chemical structures based on natural products are widely utilized in drug discovery. In this study, we focused on naphthoquinones (NPQ), a chemical core with numerous medicinal properties (e.g., antibacterial, antifungal, antiviral, anti-inflammatory, antiparasitic or antitumoral) [19]. At present, quinone derivatives are commonly used in the clinic to treat solid tumors (e.g., doxorubicin) or hematological disorders (e.g., daunorubicin). Additionally, new NPQ-based compounds are being investigated in preclinical contexts with promising results in several types of malignancies (e.g., hepatocarcinoma, melanoma, leukemia, lung cancer, breast cancer or prostate cancer) [20]. In this regard, we have previously described original NPQ derivatives [21] and NPQ-hybrid compounds [22] that exhibited effective in vitro and in vivo anti-CML properties and that have contributed to the chemical design of the compound of this study, a novel NPQ-pyrone hybrid. Pyrones have also been described to exert strong cytotoxic activity against leukemic and ovarian cancer cells [23], reduce the viability of prostate cancer cells [24] or even sensitize tamoxifen-resistant breast cancer cells [25]. Therefore, the chemical structure of NPQ-pyrone represents a promising candidate to investigate its associated antitumor mechanisms.

Herein, the present work investigates the pharmacological efficacy and molecular mechanisms involved in the action of a new NPQ-pyrone hybrid compound, 7-(3,4-dimethoxyphenyl)−10-methylbenzo[*h*]pyrano[4,3-*b*] chromene-5,6,8(7 H)-trione, named JKST6, in the context of CML. This study pays special attention to combinatorial therapy with IM and overcoming TKI resistance. Taken together, these findings provide a novel opportunity to find a drug strategy with a wider therapeutic window.

## 2. Materials and methods

### 2.1. Reagents

Imatinib (IM) and Caspases 9, 8 and 3 substrates were purchased from Calbiochem (San Diego, USA). Murine IL-3 and human IL-6 were supplied by Miltenyi Biotec (Gladbach, Germany). Z-Leu-Leu-Leu-al proteasome inhibitor was purchased from Merck (Darmstadt, Germany). In most cases, other reagents used in this research were procured by Promega (Wisconsin, USA), Roche Biochemicals (Mannheim, Germany), Sigma–Aldrich or Merck (Darmstadt, Germany).

### 2.2. Synthesis of JKST6

A mixture of 30 mg of 2-hydroxy-1,4-naphthoquinone (0.17 mmol), 54.7 mg of 3,4-dimethoxybenzaldehyde (0.34 mmol), and 42.9 mg of 4-hydroxy-6-methyl-2H-pyran-2-one (0.34 mmol) was ground for 5 min, 16.4 mg (30 mol%) of $BiCl_3$ was added, and the reaction mixture was ground again for 15 min. After incubation for 4 h at 120 °C, the resulting crude material was purified by preparative TLC using 1% DCM/MeOH as the eluent to provide 30.7 mg (42%) of JKST-6 as an amorphous orange solid. Mp: 251.3–252.5 °C. $^1$H NMR (500 MHz, $CDCl_3$) δ 2.31 (s, 3 H), 3.79 (s, 3H), 3.90 (s, 3H), 4.99 (s, 1H), 6.19 (s, 1H), 6.72 (d, *J*=8.3 Hz, 1H), 6.75 (d, *J*=1.5, 8.3 Hz, 1H), 7.11 (s, 1H), 7.61 (t, *J*=7.4 Hz, 1H), 7.78 (t, *J*=7.8 Hz, 1H),7.95 (d, *J*=7.8 Hz, 1H), 8.13 (d, *J*=7.6 Hz, 1H); $^{13}$C NMR (125 MHz, $CDCl_3$) δ 20.1 ($CH_3$), 32.6 (CH), 55.9 ($CH_3$), 56.0 ($CH_3$), 98.0 (CH), 103.4 (C), 111.2 (CH), 113.0 (CH), 117.4 (C), 119.9 (CH), 124.3 (CH), 129.8 (C), 129.9 (C), 130.0 (CH), 131.6 (CH), 134.2 (C), 135.3 (CH), 148.4 (C), 148.8 (C), 155.4 (C), 157.9 (C), 162.0 (C), 162.5 (C), 177.4 (C), 178.1 (C); EIMS *m/z* (%): 430 ([$M^+$], 100), 399 (28), 343 (34), 293 (70). HREIMS: 430.1053 (calc. for $C_{25}H_{18}O_7$ [$M^+$] 430.1053).

### 2.3. Cells

Cell lines used in the in vitro experiments were purchased from the American Type Culture Collection (ATCC). Human hematologic cell lines were grown in RPMI-1640 cell culture medium: IM-sensitive chronic myelogenous leukemia (CML) (K562, K562-GFP+, AR230); IM-resistant CML (K562-R [21], AR230-R); erythroleukemia (HEL); acute promyelocytic leukemia (HL60), acute monocytic leukemia (MOLM.13, MV4.11) and acute T cell leukemia (JURKAT). The human nonhematologic cell lines triple negative breast cancer (BT-549, MDA-MB-231, HS-578T), ER+ breast cancer (MCF7), HER2+ breast cancer (SKBR3) and endometrial adenocarcinoma (Ishikawa) were

maintained in different media. BT-549 cells were grown in RPMI-1640 medium. MDA-MB-231 and HS-578T cells were maintained in DMEM. SKBR3 cells were grown in McCoy's 5 A medium. Ishikawa cells were grown in MEM. Human peripheral blood mononuclear cells (PBMCs) were isolated from the heparin-anticoagulated blood of healthy volunteers by density gradient centrifugation with Ficoll-Paque™ PLUS (GE Healthcare Bio-Sciences AB, Sweden) and cultured in RPMI-1640 medium. Monkey nonmalignant kidney cells (Vero) and mouse monocyte macrophages (RAW 264.7) were grown in DMEM. Human mesenchymal stem cells (hMSC-TERT), kindly provided by Dr. J. M. Zapata [26], were maintained in low-glucose DMEM supplemented with 10% heat inactivated FBS. Genetically engineered KmycBT315I cells were generated by Dr. J. León [27]. Cell culture media were supplemented with 10% FBS, L-glutamine (2 mM) and PEST (50 units/ml penicillin, 50 μg/ml streptomycin), and when indicated for BT-549 cells, medium was further supplemented with 1 mM NaPyr and 10 mM HEPES. Cell culture media (RPMI-1640, DMEM) and supplements (FBS, L-glutamine, PEST) were purchased from Biowest (Nuaillé, France).

### 2.4. Cell viability assays

Immortalized cells were seeded at exponential growth density (5000 – 10,000 cells per well) in 96-well plates (BD Falcon, France), whereas PBMCs were seeded at 100,000 cells per well. Cells were treated with vehicle (0.05% DMSO) or test compounds (0.01–30 μM) for 24–72 h. Then, the tetrazolium salt 3-(4,5-methyltiazol-2yl-)− 2,5diphenyltetrazolium bromide (MTT) (Applichen, Germany) was added to cells, incubated for 2–4 h at 37 °C, and lysed in 10% SDS, and the optical density was measured at 595 nm with an iMark Microplate Reader (Bio–Rad, CA, USA) to determine the mitochondrial metabolization of the tetrazolium salt [28].

### 2.5. Wash-out assays

Cells were seeded at exponential growth (10,000 cells per well) in a 96-well plate (BD Falcon, France) and then treated with vehicle (0.05% DMSO), IM (0.03–5 μM), doxorubicin (0.1–10 μM) or JKST6 (0.1–10 μM) for 3 h. Then, drugs were removed after thorough washing with medium at 37 °C, and cells were left in drug-free medium for 48 h until cell viability was evaluated using the MTT assay [28].

### 2.6. Real-time monitoring of tumor growth (2D and 3D assays)

First, for 2D assays, CML cell lines were seeded at 5000 cells per well in a poly-L-lysine-coated 96-well plate (BD Falcon, France). Once the cell monolayer was stable after 16 h, it was treated with vehicle (0.05% DMSO) or test compound (0.03–10 μM). YOYO-1 (25 nM) (Invitrogen) was used to monitor cell membrane integrity [22]. Cell proliferation and viability were analyzed using microphotographs taken by an IncuCyte™ HD real-time imaging system (Essen BioScience, UK). The effects of each compound dose on cell growth and membrane integrity were monitored for 5 days. Then, *area under the curve* (AUC) values were plotted to analyze both the kinetics and dose effects on cell proliferation (IC50) and cytotoxicity (EC50). To support 2D assays, the effect of drugs on cell spheroids was also studied by seeding 3000 cells per well in round-bottomed, ultralow attachment, 96-well plates (ULA, Corning) [29]. Next, 24 h after spheroid formation, cells were treated with vehicle (0.05% DMSO) or drugs. The volume size and cytotoxicity of spheroids were recorded for 5 days. To calculate spheroid volume, confluence measurements were extracted using two different metrics: average phase object area ($\mu m^2$) and object count (1/image). These metrics were multiplied to obtain the total object area ($\mu m^2$), which was further used to calculate the spheroid radius ($r = \sqrt{\text{Total Object Area}/\pi}$) and the spheroid volume ($\mu m^3$) ($V = 4/3\ \pi r^3$) [29].

### 2.7. Luciferase reporter gene assay

The potential effects of drugs on STAT3 and STAT5-mediated transcriptional activity were evaluated using the Renilla Luciferase Reporter cell lines (Leeporter™ Abeomics) HEK293 and Ba/F3, respectively. Cells were seeded at 500,000 cells per well in a 12-well culture plate and 600,000 cells per well in a 24-well culture plate each. Vehicle (0.05% DMSO) or compounds (0.3–10 μM) were added before stimulation of Ba/F3 and HEK293 cells with 30 ng/ml murine IL3 (mIL3) or 10 ng/ml human IL6 (hIL6), respectively. Cells were lysed in Passive Lysis Buffer (Promega, USA), and luciferase activity was determined using a Renilla-Firefly Luciferase Assay kit (Thermo Scientific, USA) in a microplate reader (Clarity™ R2, BioTek). The results are expressed as relative luciferase units (RLUs) per mg of protein and were normalized to the results obtained in vehicle-treated cells. In parallel, MTT assays were carried out to investigate the effects of the compounds on the viability of the reporter cell lines.

### 2.8. Cell cycle and apoptosis analysis

For cell cycle studies, unsynchronized K562 cells were seeded at 300,000 cells/well in 6–well plates and treated with vehicle (0.05% DMSO) or JKST6 for 12, 24 and 48 h. After treatment, cells were harvested, washed in PBS, and fixed overnight in cold 70% ethanol. Then, the cells were resuspended in PBS containing DNAse-free RNAse (500 μg/ml) for 2 h at 37 °C, incubated with propidium iodide (PI) (5 μg/ml), and analyzed in an Accuri C6 flow cytometer (BD). A FITC-Annexin V Apoptosis Detection Kit I (BD Biosciences) was used for cell death analysis. Briefly, cells were resuspended in 100 μl of ice-cold binding buffer (10 mM HEPES pH 7.4, 140 mM NaCl, 2.5 mM $CaCl_2$), containing 5 μl of Annexin V FITC and 5 μl of PI (50 μg/ml), incubated for 15 min at room temperature, and finally, binding buffer (400 μl) was added. In both experiments, 50,000 events were collected and analyzed by fluorescence-activated cell sorting (FACS). Early apoptosis was also assessed using bisBenzimide Hoechst 33258 (Sigma–Aldrich, USA), and microphotographs were used to count the proportion of apoptotic nuclei per total nuclei observed.

### 2.9. Caspase activity assay

K562 cells were seeded at 250,000 cells/ml in 100-mm cell culture dishes and treated with vehicle (0.05% DMSO) or JKST6 (2 μM) for 6, 12 and 24 h or etoposide (30 μM) for 24 h. Next, cell pellets were resuspended in lysis buffer (50 mM HEPES, pH 7.4, 1 mM dithiothreitol, 0.1 mM EDTA, 0.1% Chaps, aprotinin, and PMSF) and centrifuged, and supernatants were utilized for the enzymatic assays. Specific peptides that are known substrates for caspase-3, −8, and −9 activities include N-acetyl-Asp-Glu-Val-Asp-p-nitroaniline (DEVDpNA), N-acetyl-Ile-Glu-Thr-Asp-p-nitroaniline (IETD-pNA), and N-acetyl-Leu-Glu-His-Asp-p-nitroaniline (LEHD-pNA) (Calbiochem, San Diego, CA), respectively. Caspase substrate cleavage leads to p-nitroaniline (pNA) release, which in turn increases its 405-nm absorbance proportionally to caspase activity. The results are expressed as the absorbance at 405 nm per mg of protein normalized to vehicle (0.05% DMSO)-treated cells.

### 2.10. Immunoblotting

Cells were seeded at 300,000 cells/ml in 100-mm dishes and treated with vehicle (0.05% DMSO) or compounds for the times and doses indicated in the figure legends. Cells were washed with cold PBS-ortovanadate (1 mM), centrifuged, and resuspended in RIPA buffer (Thermo Fisher Scientific, USA) with protease and phosphatase inhibitors (Thermo Fisher Scientific, USA). Cell lysis was achieved with 30 min of gentle agitation at 4 °C. Lysates were then centrifuged, and supernatants were collected. Protein amount was measured using a bicinchoninic acid assay (BCA) kit (BioRad). Equal protein amounts

were analyzed by SDS–PAGE and transferred to nitrocellulose membranes (Thermo Fisher Scientific, USA). Then, 5% BSA-(anti-phospho-antibodies) (Merck, Darmstadt, Germany) or 5% blotto (anti-total antibodies) (Merck, Darmstadt, Germany) diluted in Tris-buffered saline containing 0.05% Tween 20 (TBS-T) was used to block membranes for 1–2 h. Membranes were incubated overnight at 4 °C with the following primary antibodies: pTyr$^{694}$STAT5 (pSTAT5$^{Y694}$), STAT5, pTyr$^{705}$-STAT3 (pSTAT3$^{Y705}$), STAT3, pTyr$^{177}$BCR (pBCR-ABL1$^{Y177}$/pBCR$^{Y177}$), BCR, pTyr$^{412}$ABL (pBCR-ABL1$^{Y412}$), ABL, pThr$^{183}$/Tyr$^{185}$JNK (pJNK$^{T183/Y185}$), pSer$^{473}$AKT (pAKT$^{S473}$), pThr$^{308}$AKT (pAKT$^{T308}$), AKT, pThr$^{202}$/pTyr$^{204}$ERK1/2 (pERK1/2$^{T202/Y204}$), ERK1/2, pTyr$^{207}$CrkL (pCrkL$^{Y207}$), CrkL, pSer$^{240/244}$S6 (pS6$^{S240/244}$), S6, PIM1, pSer$^{780}$pRB (pRB$^{S780}$), pSer$^{807/811}$pRB (pRB$^{S807/S811}$), cyclin E, pTyr$^{15}$CDK1 (pCDK1$^{Y15}$), pSer$^{642}$Wee1 (pWee1$^{S642}$), Wee1, p27, p21, pSer$^{296}$Chk1 (pChk1$^{S296}$), pThr$^{68}$Chk2 (pChk2$^{T68}$), caspase-8, caspase-9, caspase-3 and γH2AX, which were purchased from Cell Signaling Technology (Leiden, The Netherlands). Antibodies to detect β-actin, JNK1/3 (C-17), c-MYC, cyclin B, Mcl-1 and calnexin were purchased from Santa Cruz Biotech (CA, USA). Cyclin A and BUBR1 were provided by BD Transduction Laboratories. Polyubiquitin and pSer$^{10}$ H3 (pH 3$^{S10}$) antibodies were provided by EMD Millipore. After washing with TBS-T, membranes were incubated with horseradish peroxidase-conjugated secondary antibodies (goat anti-rabbit and goat anti-mouse) that were obtained from Bio–Rad (CA, USA) for 1 h at room temperature. Finally, the protein bands were visualized using Clarity™ Western ECL Substrate (Bio–Rad, CA, USA) in the ChemiDoc XRS system (Bio–Rad, CA, USA) and were analyzed with Quantity One software (Bio–Rad, CA, USA).

### 2.11. Real-time PCR

Cells were seeded at 300,000 cells/ml in 100-mm dishes and treated with vehicle (0.05% DMSO), JKST6 (3 μM) or IM (1 μM) for 1, 3, 6 and 12 h. Then, the cells were harvested, and total RNA was isolated using PureZOL RNA Isolation Reagent (Bio–Rad, CA, USA). RNA concentration and acid nucleic purity were measured with a NanoDrop 1000 spectrophotometer (Wilmington, USA). Then, 1 μg of total RNA was used for reverse transcription to cDNA with the iScript™ kit (Bio–Rad, CA, USA) following the manufacturer's protocol. Real-time quantitative PCR (qPCR) was performed using SYBR Green PCR Master mix (Applied Biosystems, Massachusetts, USA). Exon-specific primers (Table 1) [30] were purchased from STAB VIDA (Caparica, Portugal). Gene expression was analyzed with an Mx3005P qPCR System (Agilent, CA, USA). The cycle threshold values were determined using MxPro qPCR Software (Agilent, CA, USA), and target gene expression was normalized to the GAPDH housekeeping gene. All amplifications were performed in duplicate, and Ct scores were averaged for subsequent calculations of relative expression values according to the comparative CT method for qPCR [31].

### 2.12. Drug combination assays

K562-GFP+ cells were seeded at 5000 cells per well in a 96-well plate (BD Falcon, France), and cell proliferation was analyzed using microphotographs in an IncuCyte™ HD real-time imaging system (Essen BioScience, UK). Briefly, cells were exposed to constant ratio combinations of JKST6 with IM by doubling dilutions of the individual drugs over a wide range of concentrations. Inhibition of cell proliferation, relative to untreated controls, was assigned as the effect and ranged from 0 (no cell proliferation inhibition) to 1 (100% cell proliferation inhibition). Dose-effect curves of single or combined drug treatments were plotted and analyzed by the median effect method of Chou and Talalay [32] using Calcusyn software 2.0 (Biosoft, Cambridge, UK). The analysis generated the combination index (CI) values. CI values less than 1, equal to 1, and greater than 1 indicated synergism, addition, and antagonism, respectively.

**Table 1**
Gene names and primer sequences (5′- 3′) used for real-time qPCR.

| Gene | Forward primer (5´–3´) | Reverse primer (5´–3´) |
|---|---|---|
| ***BCR*** | GGA GTC ACT GCT GCT GCT TA | ACA CTT CTT CTG CTG CTC CC |
| ***b3a2*** | GAG CGT GCA GAG TGG AGG GAG AAC ATC CGG | TGT GAT TAT AGC CTA AGA CCC GGA GCT TTT |
| ***MYC*** | CCAGCAGCGACTCTGAGG | CCAAGACGTTGTGTGTTC |
| ***PIM1*** | GCTCGGTCTACTCAGGCATC | CATTAGGCAGCTCTCCCCAG |
| ***SOCS2*** | CAG ATG TGC AAG GAT AAG CGG | CAG ATA AAG GTG AAC AGT GCC G |
| ***GAPDH*** | CCATGGAGAAGGCTGGGG | CAAAGTTGTCATGGATGACC |

### 2.13. Acute and subchronic toxicity in vivo

Acute and subchronic studies were approved by the Bioethics Committee of University of La Laguna (CEIBA 2018–0291) and the University of Las Palmas de Gran Canaria (OEBA-44/2019R1), respectively. The experiments were performed according to OECD guidelines for the testing of chemicals (N° 407; 452). The Irwin test [33] was performed in FVB male mice (Charles River Code: 207) to investigate intraperitoneal (i.p.) and oral JKST6 acute toxicity. Briefly, 12 mice were randomly distributed into 4 groups of treatments: 1) i.p. treated with vehicle (dimethilsulfoxide (DMSO): PEG400: saline; 10:40:50); 2) i.p. treated with JKST6 (10 mg/kg); 3) orally administered vehicle (DMSO: methylcellulose 0.5% (MC); 10:90); and 4) orally treated with JKST6 (50 mg/kg). Animals were treated each day for 5 consecutive days. Every day after treatment, clinical signs were gathered by two independent researchers. After 5 days, animals were euthanized by carbon dioxide overdose, necropsy allowed us to explore morphological changes in organs (liver, spleen, kidney), and every organ weight was normalized by animal body weight. The subchronic toxicity assay was performed in BALB/c (Charles River code: 028) male ($n = 10$) and female ($n = 10$) mice for 30 days. Vehicle (DMSO: PEG400: saline; 10:40:50) or JKST6 (10 mg/kg) was i.p. administered every two days. Animal welfare was assessed daily to detect any clinical signs. Body weight and food and water consumption were tracked every day of treatment. Body composition (lean, fat and fluid) was determined using an MRI scan (Bruker Minispec, Massachusetts, USA). At Day 30, mice were euthanized by isoflurane overdose followed by necropsy analysis. Blood cell counting (MS4–5, Melet Schloesing, Osny, France) and biochemistry analyses (Pointcare v2, Mano Médical, France) were also performed.

### 2.14. Statistical analysis

The data shown are the results of two to six independent experiments with at least three replicates per experimental condition. The results are expressed as the mean ± standard error of the mean (SEM) or as the mean ± standard deviation (SD) in the in vitro and in vivo assays, respectively. Differences between means of two groups were analyzed with two-tailed Student's *t*-test. One-way ANOVA followed by Bonferroni post hoc test was used to compare means from more than two groups using GraphPad Prism 8.3.0 Software (CA, USA). Statistical significance was considered when $p < 0.05$ with a 95% confidence interval. The concentration required to reduce cell viability/proliferation by 50% (IC50) or to induce cytotoxicity by 50% (EC50) was graphically determined using the curve fitting algorithm of GraphPad Software. For the in vivo experiments, equal numbers of animals were selected and randomly distributed into each treatment group. The minimal number of animals to be used was determined with statistical power and sample size analysis using G Power 3.1 Software (Düsseldorf, Germany) and followed the OECD recommendation (N°407).

## 3. Results

### 3.1. Antitumoral efficacy of JKST6 on human leukemia cells

JKST6 was identified within a naphthoquinone-enriched library by high-throughput cell-based phenotypic screening (Fig. 1**A**). First, the antitumoral effects of JKST6 were evaluated by MTT assay. Interestingly, JKST6 showed higher efficacy against cell lines derived from hematological malignancies (i.e., K562, MOLM-13, HL-60, HEL, MV 4.11, JURKAT cell lines) than against breast cancer-derived cells (i.e., BT-549, MDA-MB-231, HS-578 T) or nonmalignant cells (i.e., RAW 264.7, Vero, hMSCs, and PBMCs) (Table 2). The cytotoxicity of JKST6 on quiescent human PBMCs was 4-fold lower than that in K562 cells (Table 2). Remarkably, low concentrations (1 and 3 μM) of JKST6 showed no significant effect on PBMC viability compared to K562, whereas doxorubicin, a chemotherapeutic agent used in a broad spectrum of tumor types, reduced PBMC and K562 viability with similar potency (Fig. 1**B**). The low toxicity displayed by JKST6 in vitro was also validated in vivo. JKST6 (10 mg/kg) was administered to mice in acute (5 days, data not shown) and subchronic (30 days) toxicity assays. The results confirmed that the clinical signs, blood cell populations or biochemical parameters of JKST6-treated animals were mostly unaffected when compared with those of the vehicle-treated group (Supplementary Figure 1, Supplementary Tables 1–2).

As shown in Table 2, JKST6 exhibits potent antitumoral effects in K562 cells, a model of human CML. Thus, we further investigated the irreversible effects of a short exposure (3 h) of K562 cells to JKST6. IM and doxorubicin were also analyzed in this set of experiments. The data revealed that JKST6 (IC50 = 1.57 ± 0.28 μM) and doxorubicin (IC50 = 0.74 ± 0.12 μM) maintained their antitumoral potency after short exposure (3 h) of K562 to the drugs followed by 48 h of wash-out, whereas IM reduced its antitumoral effect (IC50 > 5 μM) (Fig. 1**C**). These results suggest that short and transient exposure to JKST6 is enough to maintain, at least for 48 h, the inhibitory effects induced by

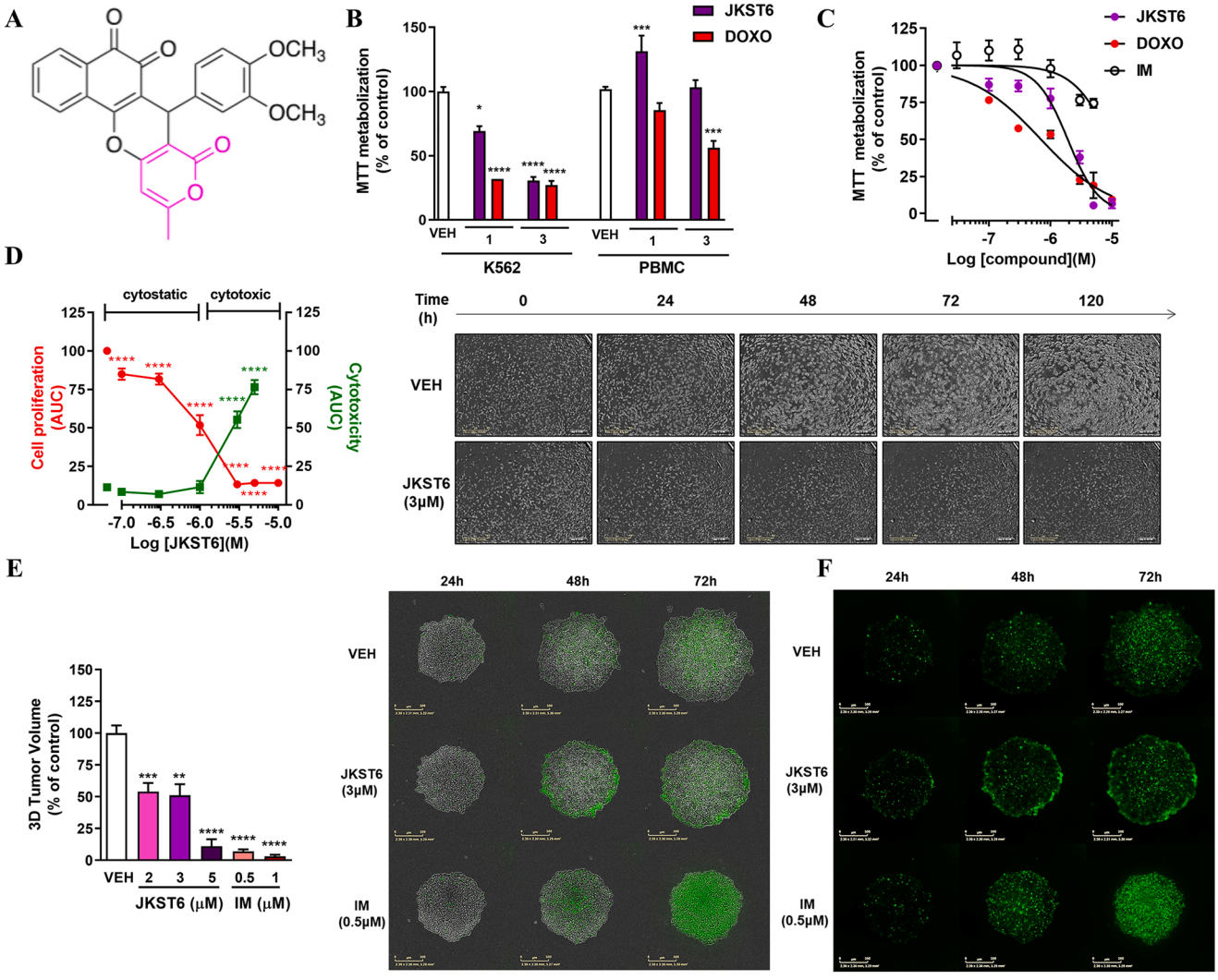


**Fig. 1. Antitumoral efficacy of JKST6 on human leukemia cells. (A)** Chemical structure of JKST6; the pyrone group is highlighted in color. **(B)** Cell viability measured in K562 and PBMC cells incubated with JKST6 or doxorubicin (DOXO) (both at 1 and 3 μM) for 24 h. **(C)** Cell viability measured in K562 cells exposed to graded concentrations (0.01–10 μM) of JKST6 (●), DOXO (●) or IM (○) for 3 h followed by wash-out steps. **(D)** Proliferation and cytotoxicity in K562 cells treated with vehicle (VEH; 0.05% DMSO) or JKST6 (0.01–10 μM) for 5 days. Data represent the area under the curve (AUC) by JKST6 dose **(left panel)** and representative microphotographs of exponentially growing K562 cells under VEH or JKST6 (3 μM) conditions at 0, 24, 48, 72 and 120 h **(right panel)**. **(E)** 3D cultures of K562 cells exposed to VEH, JKST6 (2, 3, and 5 μM), or IM (0.5 and 1 μM) for 5 days. Representative microphotographs of tumor spheroids in the absence (VEH) or presence of compounds (3 μM JKST6 and 0.5 μM IM) at 24, 48 and 72 h **(right panel)** and quantification of tumor volume calculated as a percentage of the control **(left panel)**. **(F)** Representative green fluorescence microphotographs of YOYO-1-labeled K562 tumor spheroids in the absence (VEH) or presence of compounds (3 μM JKST6 and 0.5 μM IM) at 24, 48 and 72 h. Figures are representative of at least 3 independent experiments, each performed in triplicate. Statistical significance was assessed using one-way ANOVA with Bonferroni post hoc test. *$P < 0.05$; ** $P < 0.01$; ***$P < 0.001$; ****$P < 0.0001$ versus VEH-treated cells.

**Table 2**
Effects of JKST6 on cancer (blood and solid tumors) and normal cell viability.

| Cell line | IC50 (μM; mean ± SEM) |
|---|---|
| K562 | 0.66 ± 0.29 |
| MOLM-13 | 0.71 ± 0.20 |
| HL-60 | 0.88 ± 0.09 |
| HEL | 1.02 ± 0.16 |
| MV4.11 | 1.04 ± 0.08 |
| ISHIKAWA | 1.43 ± 0.19 |
| JURKAT | 1.69 ± 0.01 |
| BT-549 | 1.99 ± 0.87 |
| MCF10A | 2.27 ± 0.16 |
| MDA-MB-231 | 2.70 ± 0.16 |
| MCF7 | 3.18 ± 0.21 |
| HS-578T | 3.25 ± 1.20 |
| hMSC-TERT | 4.61 ± 1.27 |
| SKBR3 | 4.68 ± 0.62 |
| RAW 264.7 | 5.13 ± 0.95 |
| PMBC | 5.68 ± 0.9 |
| VERO | 6.44 ± 2.02 |
| EVB lymphocytes | > 10 ± ND |

Cells were treated with vehicle (0.05% DMSO) or JKST6 (0.01–10 μM) for 24–72 h. Then, cell viability was assessed by MTT assay as described in Material and Methods. ND: not determined.

this new product on K562 cell viability.

Furthermore, 2D real-time monitoring of K562 cell growth permitted to discern cytostatic (lower than 1 μM) and cytotoxic (higher than 3 μM) JKST6 doses in a long-term experiment (5 days) (Fig. 1**D**). Instead, IM showed a cytostatic effect around 0.25 μM and cytotoxic effects at doses higher than 1 μM (data not shown). As a representative image, bright-field microphotographs of K562 cells exposed to 3 μM JKST6 or vehicle are shown (Fig. 1**D**). In addition, kinetic studies showed the rapid antiproliferative effects of JKST6 (IC50 = 0.91 μM at 12 h) compared to IM (IC50 > 5 μM at 12 h) (Supplementary Figure 2). To better mimic a real tumor in vivo, 3D spheroid experiments with K562 cells were performed. Notably, JKST6 significantly reduced spheroid growth compared to vehicle-treated K562 cells (Fig. 1**E**). Moreover, JKST6 cytotoxicity especially affected the K562 spheroid perimeter at short times (48 h) when compared to IM cytotoxicity (Fig. 1**F**). Taken together, these results show that JKST6 has a rapid and long-term antitumor effect in CML cells and that its low toxicity in healthy cells might be clinically relevant.

### 3.2. JKST6 inhibits cell cycle entry and induces apoptosis in human CML cells

To further evaluate the manner in which JKST6 suppresses K562 cell growth, we performed cell cycle profiles and apoptosis studies by flow cytometry. As shown in Fig. 2**A-B**, all doses of JKST6 promoted a significant increase in the subG1 phase, accompanied by a corresponding decrease in the G0/G1 phase, especially after 24 and 48 h of drug exposure. Consistently, changes in proteins involved in cell cycle regulation were also observed after JKST6 treatment (Fig. 2**C**). In particular, the compound markedly reduced the phosphorylation of pRB, a protein that controls cell cycle entry, at only 6 h posttreatment, whereas Cyclin E, which is associated with G1-S transition, showed a peak at 24 h followed by a reduction at 48 h. Proteins that have key roles in the S and M phases were also altered by JKST6. Thus, JKST6 increased Cyclin A and B levels after 48 h of treatment. We also observed that Wee1, a checkpoint protein that negatively controls mitosis entry, was phosphorylated at short times of compound exposure. A reduction in the activation of H3, a histone that is phosphorylated in different patterns in mitosis, was also evident from 6 to 48 h posttreatment. Moreover, certain negative regulators of mitosis progression (pCHK1, pCHK2, p21) were activated after JKST6 treatment (Fig. 2**C**).

The increase in subG1 phase implies an enhanced number of hypodiploid cells, which in turn represent dead cells. To identify the mechanism of death induced by JKST6, we performed apoptosis assays that measured Annexin V and propidium iodide (PI) staining using doses and time points used for cell cycle analysis. Significant time- and dose-dependent increases in Annexin V-positive cells were detected (Fig. 3**A**), along with an increase in the number of apoptotic nuclei 24 h after JKST6 treatment (Fig. 3**B**). Apoptotic death can be dependent or independent of the activity of certain caspases. Therefore, to better understand the death mechanisms activated by JKST6, different initiator and effector procaspases, as well as poly (ADP-ribose) polymerase (PARP), were studied. As shown in Fig. 3**C-D**, JKST6 treatment induced the cleavage and activity of procaspases 8 and 9 at 12 h, whereas the cleavage of procaspase-3 and PARP was detected from 12 to 48 h after treatment. Moreover, phosphorylation of the DNA double strand breaks marker H2AX was detected just 6 h after treatment, which, together with Chk1 and Chk2 activation, indicated the presence of genetic damage. Finally, Mcl-1, a pro-survival Bcl2 family protein, was induced after short-term JKST6 treatment (Fig. 3**C**). Taken together, these data revealed that JKST6 reduces K562 cell growth, inhibits cell cycle entry, causes DNA damage, and induces apoptosis.

### 3.3. JKST6 inhibits BCR-ABL1/STAT5 and modulates associated survival pathways in human chronic myelogenous leukemia

To determine whether JKST6 effectively targets the BCR-ABL1/STAT5 signaling pathway, protein and mRNA expression analyses were performed in K562 cells. Interestingly, hyperphosphorylation of BCR-ABL1 ($p^{Y412}$ and $p^{Y177}$) was efficiently inhibited by JKST6 (3 μM at 3 h) (Fig. 4**A**). However, this finding was concomitant with a reduction in the chimeric BCR-ABL1 protein measured in ABL and BCR domains, whereas BCR and c-ABL wild-type proteins remained practically unaltered after JKST6 treatment (Fig. 4**A**). Importantly, constitutive phosphorylation of $pSTAT5^{Y694}$ was inhibited after JKST6 treatment without altering total STAT5 levels (Fig. 4**A**). To explore the mechanism that causes a reduction in BCR-ABL1 after JKST6 treatment, the levels of polyubiquitinated proteins were studied. The results showed evident increases in ubiquitinated proteins after short-term treatments (0.5, 1 and 3 h) compared to vehicle-treated cells (Fig. 4**A**). The extent of the posttranslational effect caused by JKST6 was studied using a proteasome inhibitor (MG132) to block proteolytic activity [34] prior to compound addition, as shown in Fig. 4**B**. Cells were pretreated with MG132 for 2 h before JKST6 treatment for another 1, 3 or 6 h. First, JKST6 alone caused a peak in ubiquitinated proteins at 1 h after treatment, as previously observed. MG132 induced an evident increase in ubiquitinated proteins compared with the vehicle at all time points. Moreover, MG132 (2 h) followed by JKST6 resulted in the potentiation of ubiquitinated proteins after 1 and 3 h of treatment and, importantly, partially prevented the JKST6-induced downregulation of BCR-ABL1 protein at 1 h. Surprisingly, the mixture enhanced the reduction in total oncoprotein levels after 3 and 6 h of treatment (Fig. 4**B**).

The expression of other key components involved in BCR-ABL1/STAT5 signaling was analyzed, including CrkL [35], c-MYC and PIM1 [4]. As shown in Fig. 4**C**, all these proteins were also downregulated by JKST6 treatment, thus indicating a blockage of the BCR-ABL1/STAT5 downstream cascade by the compound. To understand whether STAT transcription factor activity may be downregulated by JKST6, Renilla luciferase assays were performed. Notably, in the BaF3 reporter cell line, JKST6 inhibited IL3-induced STAT5 luciferase activity (IC50 = 4.26 ± 0.05 μM) without disturbing cell viability (IC50 = 9.58 ± 0.58 μM) (Fig. 5**A**). Although less potent (IC50 = 7.18 ± 1.48 μM), JKST6 treatment also decreased IL6-induced STAT3 transcriptional activity in the HEK293 reporter cell line without causing toxicity (IC50 > 10 μM) (Fig. 5**B**). RNA analysis was performed to assess whether JKST6 provokes gene expression inhibition alongside protein content reduction of BCR-ABL1 using two different primer pairs that amplify exons 12 and 13 of BCR *(BCR)* and the junction region of

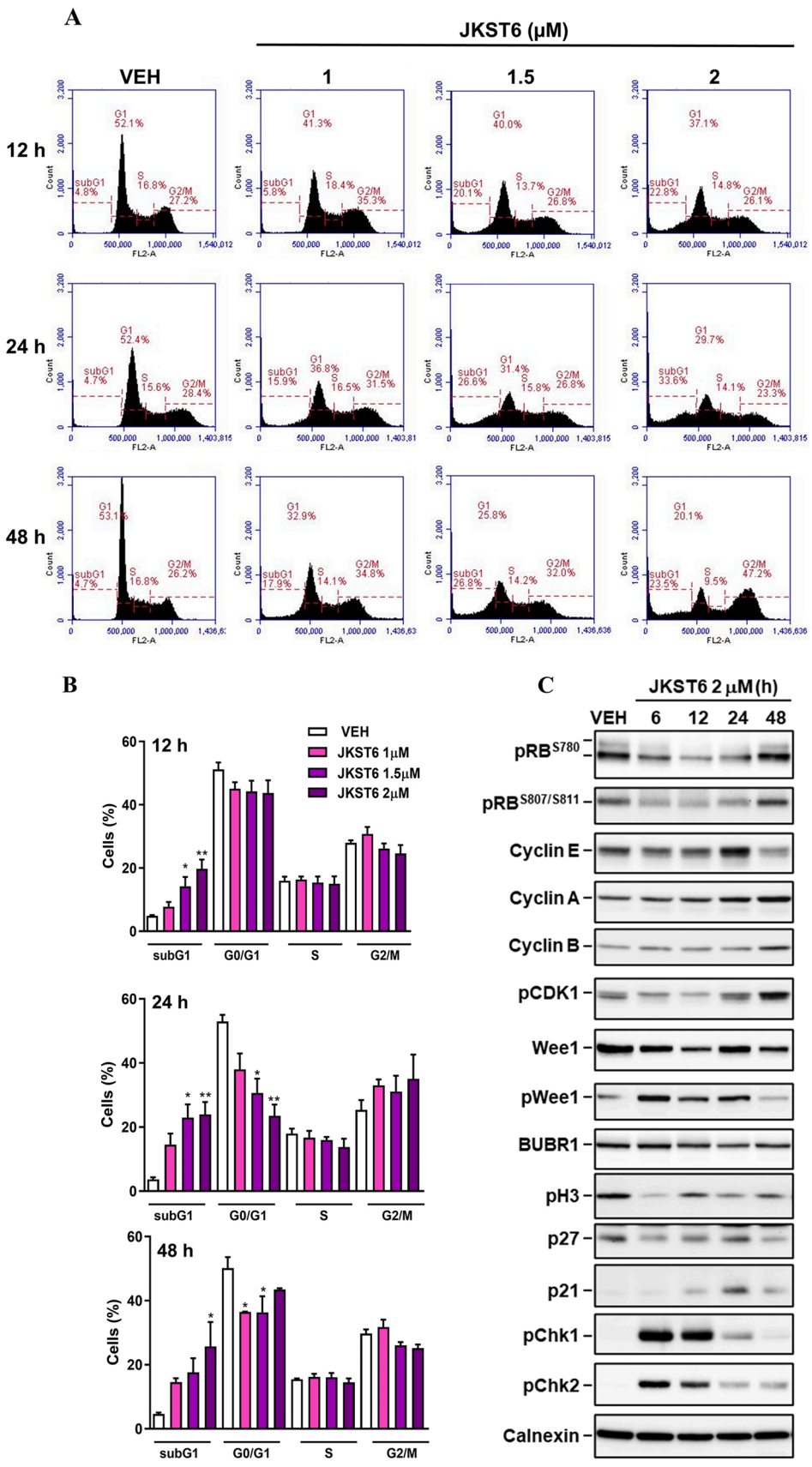


**Fig. 2. JKST6 blocks cell cycle entry in human chronic myelogenous leukemia cells. (A)** Cell cycle studies in K562 cultures treated with vehicle (VEH; 0.05% DMSO) or different doses of JKST6 (1, 1.5 and 2 μM) for 12, 24 and 48 h. Representative FACS images classifying cells according to their profiles in subG1, G0/G1, S, and G2/M phases. **(B)** Quantification of the percentages of cells in the different subregions at each time point shown in Panel A. Figures are representative of three independent experiments, each performed in triplicate. **(C)** Cell cycle protein expression analysis by immunoblotting assay from total cell lysates of K562 cells exposed to JKST6 (2 μM) for 6, 12, 24 and 48 h. Calnexin was used as a loading control. Figures are representative of two independent experiments. Statistical significance was assessed using one-way ANOVA with Bonferroni post hoc test. $*P < 0.05$; $**P < 0.01$versus VEH-treated cells.

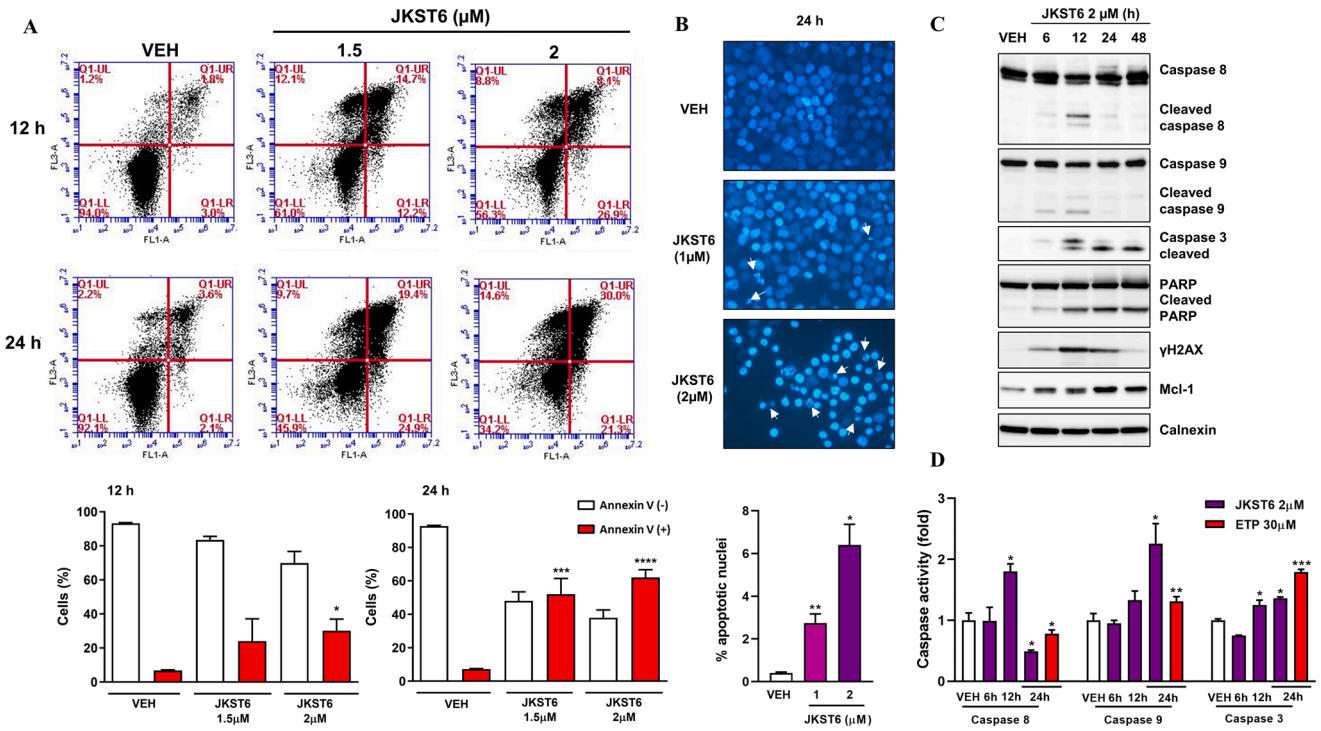


**Fig. 3. JKST6 induces apoptosis in K562 cells. (A)** Analysis of apoptosis in K562 cells treated with vehicle (VEH; 0.05% DMSO) or JKST6 (1, 1.5 and 2 μM) for 12 and 24 h using the Annexin V-FITC apoptosis detection kit. Representative FACS images of the measurement of phosphatidylserine translocation to the cell surface **(upper panel)** and quantification of the percentages of Annexin V (-) and Annexin V (+) cells at each time point **(lower panel)**. Graphs are representative of three independent experiments, each performed in triplicate. **(B)** Fluorescence microscopy microphotographs of K562 cells stained with bisbenzimide to identify apoptotic nuclei after JKST6 (1 μM and 2 μM) treatment for 24 h. Arrows mark apoptotic cells with condensed chromatin **(upper panel)**, with percentage representation of apoptotic nuclei **(lower panel)**. **(C)** Immunoblotting analysis of proteins involved in apoptosis from total cell lysates of K562 cells exposed to VEH or JKST6 (2 μM) for 6, 12, 24 and 48 h. Calnexin was used as a loading control. Representative images from two independent experiments are shown. **(D)** Analyses of caspase-8, − 9, and − 3 activities determined in K562 cells exposed to VEH, JKST6 (2 μM) or etoposide (ETP) (30 μM) for 6, 12 and 24 h. The results represent the fold increase in caspase activity compared to VEH. Figures are representative of two independent experiments, each performed in duplicate. Statistical significance was assessed using one-way ANOVA with the Bonferroni post hoc test. $^{*}P < 0.05$; $^{**}P < 0.01$; $^{***}P < 0.001$; $^{****}P < 0.0001$ versus VEH-treated cells.

the oncoprotein (*b3a2*). In addition, STAT5 target genes (*MYC* and *PIM1*) were also studied (Fig. 5**C**). Notably, the relative gene expression profile showed a different pattern of suppression than the one detected in the immunoblot assays, highlighting the earlier decrease in BCR-ABL1 protein levels (3 h posttreatment) followed by later reductions in *BCR* and *b3a2* mRNA levels (12 h posttreatment). Sustained *MYC* mRNA downregulation was produced by JKST6, whereas *PIM1* downregulation was observed at short times followed by enhanced expression at 12 h.

Finally, alternative survival pathways also modulated by BCR-ABL1 in CML were analyzed [7]. Accordingly, JKST6 inhibited the phosphorylation of Src family kinases at 12 h, as well as P38-MAPK and S6, and transiently augmented AKT and JNK phosphorylation when compared to nontreated K562 cells (Fig. 6**A-B**). ERK1/2 phosphorylation seemed to be increased at 30 min and remained augmented until 12 h after treatment (Fig. 6**A**). Therefore, these results suggest that JKST6 negatively modulates the BCR-ABL1/STAT5 pathway in K562 cells.

### 3.4. JKST6 potentiates imatinib-induced antiproliferative effects and STAT5 inhibitory activity

Drug combinations allow the use of lower doses that hinder drug resistance development or promote more effective target inhibition [21]. Hence, to evaluate whether JKST6 enhances the antiproliferative effect of IM, dose–response synergistic assays combining both compounds were performed. For these studies, IM-sensitive K562-GFP+ cells were treated with different doses of JKST6 and IM, following a constant ratio combination design [7.5(JKST6):1(IM)] at different time points. Very interestingly, we found a significant increase in IM potency compared with IM alone when combined with JKST6 at all time points (Fig. 7**A**). Furthermore, isobologram and Chou-Talalay analyses of the combination index (CI) [32] showed that JKST6 and IM acted synergistically in inducing antiproliferative effects (CI (24 h) for ED50 = 0.42 ± 0.10 and CI (24 h) for ED75 = 0.38 ± 0.11)/(CI (48 h) for ED50 = 0.55 ± 0.16 and CI (48 h) for ED75 = 0.46 ± 0.13) (Fig. 7**B**). Importantly, synergistic effects of the JKST6-IM combination on $pSTAT5^{Y694}$ levels were also observed. Thus, when K562 cells were treated with different combination doses of IM (0.03 or 0.05 μM) and JKST6 (0.5 or 1 μM) for 3 h, the phosphorylation of STAT5 at $Y^{694}$ was significantly more inhibited than when cells were treated with individual compounds (Fig. 7**C**).

### 3.5. JKST6 reduces cell growth, cell viability and the BCR-ABL1/STAT5 signaling pathway in imatinib-resistant cells

Resistance to IM treatment has been associated, among other mechanisms, with the T315I-BCR-ABL1 mutation, BCR-ABL1 overexpression or antidrug transporters [12]. For this reason, the capacity of JKST6 to extend its antitumoral effect to IM-resistant cells was studied in a series of viability assays, as indicated in Table 3. First, IM-resistant and IM-sensitive K562 cells (K562-R and K562, respectively) were treated with increasing concentrations of IM or JKST6 for 48 h. As we previously described [22], the IM-IC50 was approximately 20 times higher in K562-R cells (3.86 ± 0.37 μM) than in K562 cells (0.14 ± 0.05 μM), whereas JKST6 displayed similar antitumoral efficacy in both cell line models (IC50 = 1.03 ± 0.11 μM and IC50 = 0.66 ± 0.09 μM in K562-R

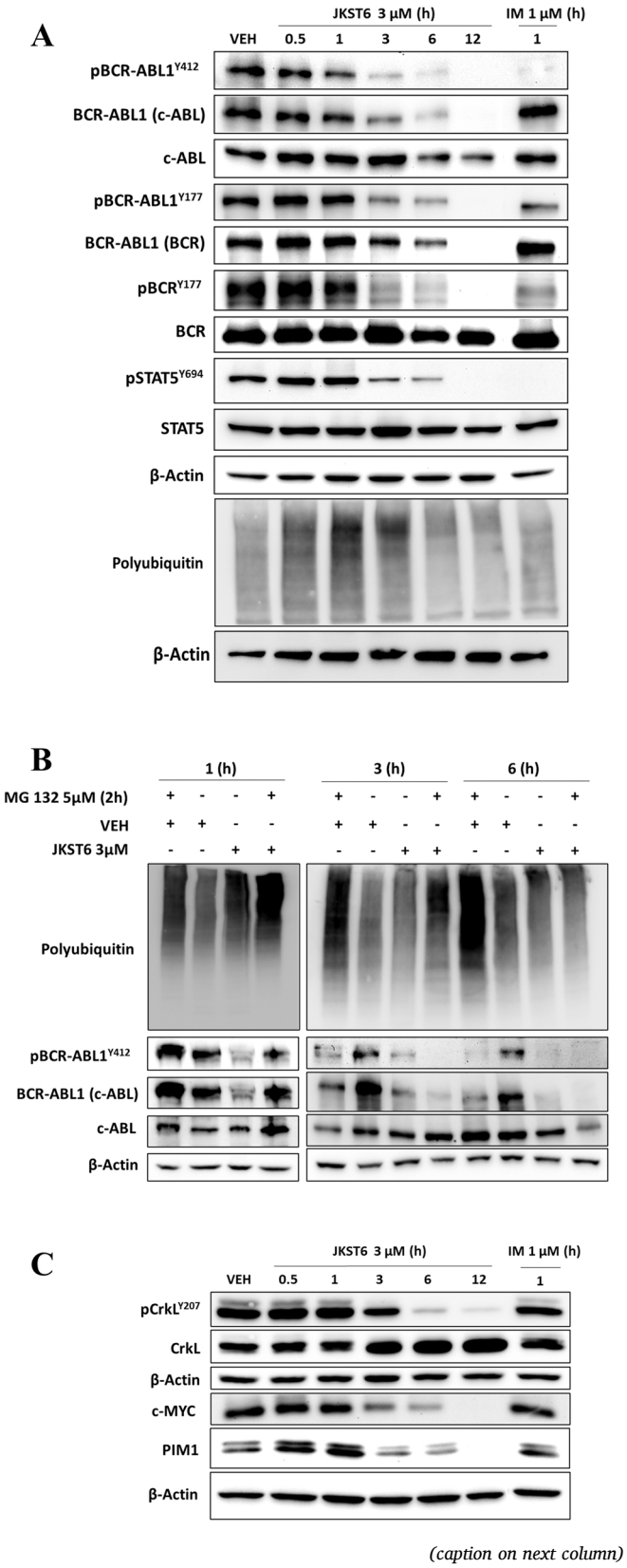


*(caption on next column)*

**Fig. 4. JKST6 suppresses the BCR-ABL1/STAT5 signaling pathway and modulates posttranslational mechanisms associated with protein degradation. (A)** Immunoblotting detection of phosphorylated ($pY^{412}$)/($pY^{177}$) and total levels of BCR-ABL, BCR, c-ABL, STAT5 and polyubiquitin from whole-cell extracts of K562 cultures previously treated with vehicle (VEH; 0.05% DMSO), JKST6 (3 μM) or IM (1 μM) for the indicated times. **(B)** Immunoblotting detection of phosphorylated ($pY^{412}$) and total levels of BCR-ABL1 and c-ABL and polyubiquitin from total cell lysates of K562 cells pre-exposed to the proteasome inhibitor MG132 or VEH for 2 h followed by VEH or JKST6 (3 μM) treatment for the indicated times. **(C)** Immunoblotting analysis of BCR-ABL1/STAT5 axis-downstream proteins ($pY^{207}$-CrkL, CrkL, PIM1, c-MYC) from cell lysates of K562 cells treated with VEH, JKST6 or IM for the indicated times. β-actin was used as a loading control. Representative images from three independent experiments are shown.

and K562 cells, respectively) (Fig. 8**A**). Remarkably, a low JKST6-IC50 value was obtained in a K562-transfected clone expressing the T315I-BCR-ABL1 mutation [27], recognized as a key mechanism of IM resistance (Table 3). However, IM treatment was clearly ineffective in these cells (Table 3). Additionally, the AR230 cell line is a CML model with IM-sensitive (AR230) and IM-resistant (AR230-R) clones which carry a 230-kDa BCR-ABL1 fusion variant and exhibits IM resistance through oncoprotein overexpression [36], showing 12 times lower responsiveness to IM (AR230-R) than its IM-sensitive counterpart, AR230 (1.89 ± 0.55 μM and 0.15 ± 0.02 μM, respectively). In contrast, the IC50 values obtained for JKST6 were similar in both cell clones (1.52 ± 0.31 μM and 1.57 ± 0.49 μM in AR230-R and AR230 cells, respectively) (Table 3).

To examine the irreversible effects of JKST6 on IM-resistant cells, wash-out experiments were performed by short-term exposure (3 h) of K562-R cells to JKST6, doxorubicin or IM followed by drug removal from the media for 48 h. As expected, IM was ineffective (IC50 >5 μM), whereas both JKST6 (IC50 = 2.86 ± 0.17 μM) and doxorubicin (IC50 = 2.12 ± 1.12 μM) were able to significantly reduce the viability of K562-R cells (Fig. 8**B**). Predictably, live cell imaging of K562-R proliferation in long-term experiments (5 days) showed that IM was less potent on K562-R cells (IC50 = 4.55 ± 1.31 μM) than on K562 cells (IC50 = 0.24 ± 0.2 μM), whereas JKST6 remained equally effective in both cases (IC50 = 1.07 ± 0.19 μM versus IC50 = 0.75 ± 0.10 μM) (Fig. 8**C**). For a pathophysiological approach, 3D spheroid live-cell imaging assays were performed in AR230-R cells and showed a JKST6 dose-time-dependent volume shrinkage, whereas IM was unable to exert a significant effect on tumor volume (Fig. 8**D**). Moreover, JKST6 caused rapid (24 h) damage to peripheral cells, while IM cytotoxicity was visible at 24 and 48 h but seemed to be ineffective at 72 h (Supplementary Figure 3**A**). Finally, due to the importance that BCR-ABL1 overexpression has in IM resistance, we investigated whether JKST6 maintained its molecular mechanism of action in AR230-R cells using AR230 cells as a control (Fig. 9**A**). Notably, 3 μM JKST6 effectively reduced the levels of total BCR-ABL1 in both clones and thus BCR-ABL1 phosphorylation ($pY^{177}$, $pY^{412}$) at just 3 h after treatment (Fig. 9**A**). Likewise, hyperphosphorylation of STAT5 (higher in AR230-R cells) and PIM1 and c-MYC protein expression levels were significantly inhibited at 3 h of JKST6 exposure. In contrast, IM was considerably less efficient in inhibiting BCR-ABL1 and STAT5 phosphorylation in IM-resistant AR230-R cells (Fig. 9**A-right panel**) than in their IM-sensitive counterparts (Fig. 9**A-left panel**). Moreover, JKST6 induced γH2AX (at 3, 6 and 12 h after treatment) and reduced CrkL phosphorylation (at 6 and 12 h after treatment) to a similar extent in both cell clones. However, IM was not able to induce γH2AX phosphorylation in AR230-R cells (Fig. 9**A-right panel**). To investigate whether the reduction in BCR-ABL1 protein levels by JKST6 could contribute to restoring the

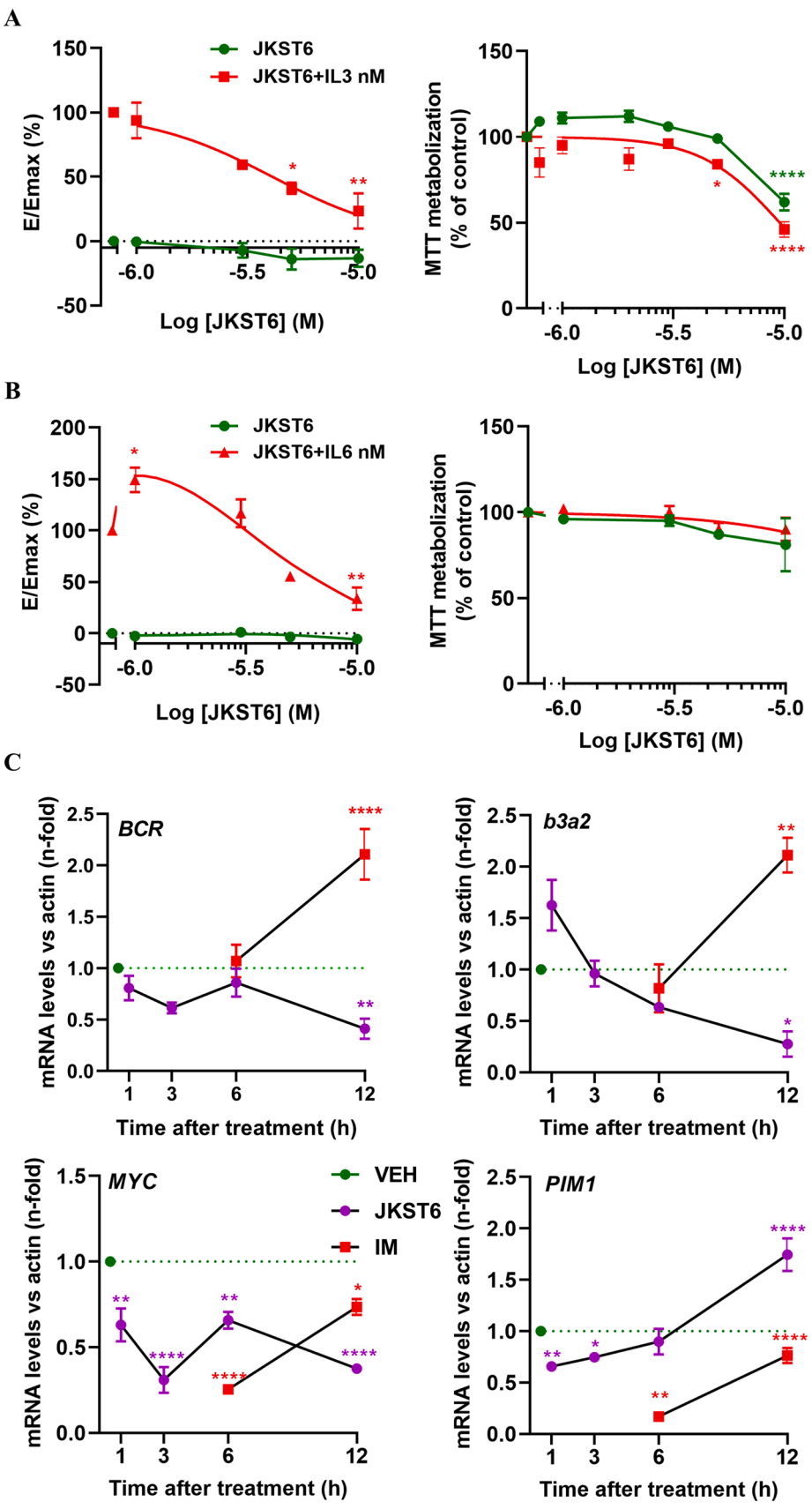


**Fig. 5. JKST6 inhibits STAT5- and STAT3-dependent transcription and *BCR-ABL1* oncogene and STAT5-target gene expression. (A)** STAT5 transcriptional activity measured by luciferase assay in the BaF3 reporter cell line exposed to vehicle (VEH; 0.05% DMSO) or increasing concentrations of JKST6 (0.3–10 μM) for 4 h followed by STAT5 transcriptional activity induction (interleukin mIL3 (30 ng/ml), ■) for 16 h in contrast with basal signal (not induction, ●) **(left panel).** Cell viability measured in BaF3 cells analyzing the same JKST6 doses and time points as in the luciferase assay **(right panel). (B)** STAT3 transcriptional activity measured in the Renilla luciferase HEK293 reporter cell line exposed to VEH or increasing concentrations of JKST6 (0.3–10 μM) for 4 h followed by STAT3 transcriptional activity induction (interleukin hIL6 (10 ng/ml), ▲) compared with basal signal (not induction, ●) **(left panel).** Cell viability measured in HEK293 cells analyzing the same JKST6 doses and time points as in the luciferase assay **(right panel).** Luciferase activity was measured as explained in the Materials and Methods. The maximal effect of luciferase activity (100%) was assigned to VEH-treated cells stimulated with (mIL3 or hIL6) interleukin, and the rest of the dose effects were normalized by this value. Figures are representative of at least two independent experiments, each performed in duplicate. Statistical significance was assessed using one-way ANOVA with Bonferroni post hoc test. $^{*}P < 0.05$; $^{**}P < 0.01$; $^{****}P < 0.0001$ versus VEH-treated and mIL3 **(A)** or hIL6 **(B)**-stimulated cells. **(C)** mRNA expression analysis by qPCR of BCR-ABL1/STAT5 axis-target oncogenes *(BCR; b3a2; PIM1, c-MYC* and the housekeeper *GAPDH)* in K562 cells treated with VEH (●), JKST6 (3 μM, ●) or IM (1 μM, ■) for the indicated times. Data are presented as the mean ± SEM of three independent experiments, each performed in duplicate. Statistical significance was assessed using one-way ANOVA with Bonferroni post hoc test. $^{*}P < 0.05$; $^{**}P < 0.01$; $^{****}P < 0.0001$ versus VEH-treated cells.

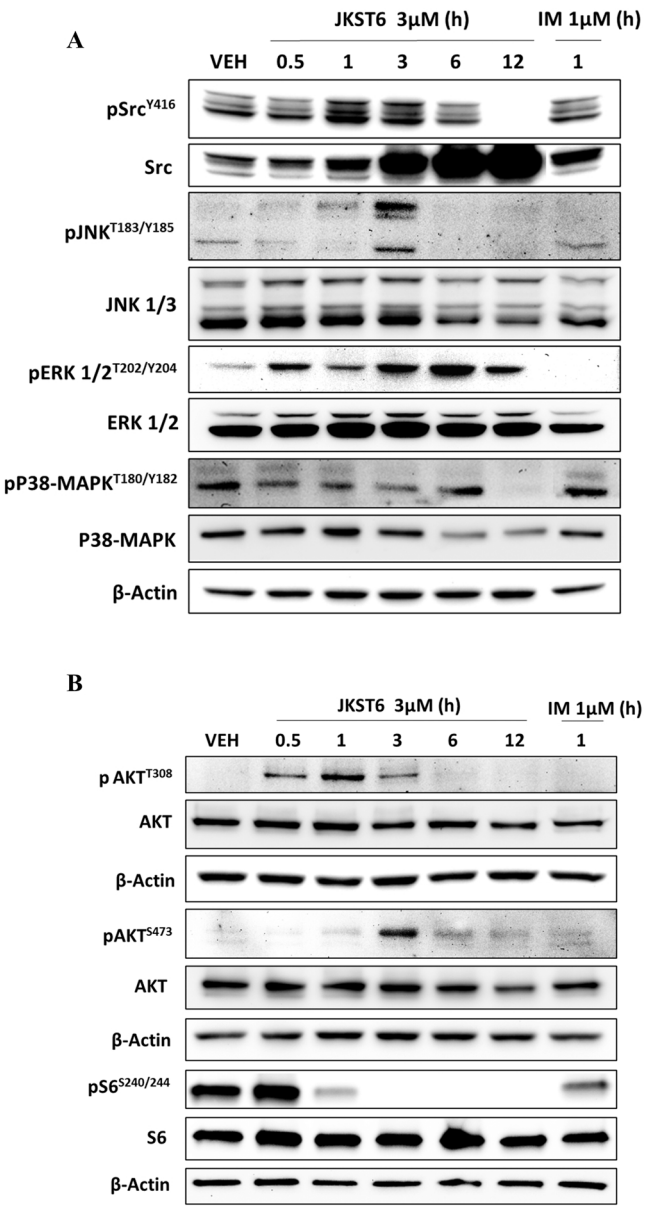


**Fig. 6. JKST6 modulates important alternative survival pathways in CML.** Protein expression analysis by immunoblotting assay of phosphorylated and total key signaling proteins **(A)** (pY$^{416}$-Src, Src, pT$^{183}$/Y$^{185}$-JNK, JNK1/3, pT$^{202}$/Y$^{204}$-ERK1/2; ERK1/2; pT$^{180}$/Y$^{182}$-p38-MAPK, p38-MAPK; **(B)** pT$^{308}$-AKT, AKT, pS$^{473}$-AKT, AKT, pS$^{240/244}$-S6, S6) from whole-cell extracts of K562 cells exposed to vehicle (VEH; 0.05% DMSO), JKST6 (3 μM) or IM (1 μM) for the indicated times. β-actin was used as a loading control. Images are representative of at least two independent experiments.

sensitivity of AR230-R cells to IM, cells were pre-exposed to vehicle or JKST6 for 3 h, followed by wash-out, and the dose effect on IM was evaluated at 48 h (Fig. 9**B**). Of interest, IM potentiated its effects by 14 times when cells were pretreated with JKST6 (IC50 = 0.175 ± 0.003 μM) compared to vehicle pre-exposed cells (IC50 = 2.17 ± 0.17 μM). JKST6 inhibited the same key proteins involved in the BCR-ABL1/STAT5 pathway in the AR230 and K562 CML models; thus, the effect of JKST6 on mRNA expression was analyzed in K562-R cells (Fig. 9**C**). JKST6 provoked a different modulatory pattern of mRNA expression when compared to the protein levels, according to previous studies in K562 cells. The gene expression of *SOCS2*, a negative regulator of the JAK/STAT pathway associated with CML progression to the aggressive blast phase [37], was also assessed in both K562 and K562-R cells (Fig. 9**C**). IM treatment reduced the expression of *SOCS2,* whereas JKST6 provoked a peak of induction at 6 h in both cell lines. In summary, JKST6 displays the same potential for inhibiting the BCR-ABL1/STAT5 signaling pathway and its downstream effectors in both IM-resistant and IM-sensitive cells. Importantly, JKST6 might rescue the sensitivity of IM-resistant CML cells to IM.

## 4. Discussion

NPQ derivatives have emerged as promising therapeutic agents in cancer in the last decade. The present work reveals the pharmacological efficacy of a novel NPQ-pyrone hybrid, JKST6, in human CML cells and shows the molecular mechanisms responsible for its potent antitumoral effects. Interestingly, we show how the JKST6 compound is effective in overcoming imatinib resistance in a wide range of resistant cells with known resistance mechanisms present in CML patients; thus, it is a promising new pharmacological tool that could improve current therapeutic opportunities.

Antiproliferative capacity and low toxicity are two crucial aspects of a clinically relevant antitumoral drug. Therefore, the antiproliferative effects of JKST6 in hematological and nonhematological cancer and normal cells were investigated. Our data show that JKST6 effectively inhibits the growth of human leukemia cells with high potency (i.e., sub μM IC50 values in K562 and MOLM-13) compared to solid tumor cells (e.g., BT-549, MDA-MB-231, MCF7). Remarkably, the viability of nonmalignant cells was hardly affected by JKST6 treatment, which agrees with the low toxicity observed by compound administration in vivo. These results suggest that JKST6 may find specific molecular targets in myeloid-derived cancer cells, which makes them more sensitive to the compound than other leukemias or nonhematological cancer cells. JKST6 displays rapid antiproliferative activity and longer-lasting antitumoral effects on CML cells after short drug exposure when compared to the BCR-ABL1 inhibitor IM. These findings outline a JKST6 durable action that is normally associated with ligand-target covalent bonds, long drug-target residence, or posttranslational effects after drug-target union [38,39]. Interestingly, JKST6 shows a wide window between cytostatic and cytotoxic doses, coinciding with reported studies of pyrones that display elevated antiproliferative over cytotoxic activity [40]. Moreover, the antitumor efficacy of JKST6 was validated in CML cell spheroids, a culture system that faithfully reproduces tumor biology in vivo. In fact, differences between 2D monolayer and 3D cultures have been widely reported, and some of them include signal transduction, gene and protein expression, cell differentiation or drug sensitivity [41]. Furthermore, recent studies have found that leukemic cells are metabolically more stable in 3D than in 2D standard cultures, where they are prone to undergo phenotypic changes with passage [42]. Thus, the growth inhibition of CML spheroids induced by JKST6 in vitro may represent a valid approach for its potential antitumor efficacy in vivo [41].

It has been reported that NPQ-based derivatives and hybrids are able to induce antiproliferative effects on CML cells through diverse mechanisms, including oxidative stress, cell cycle arrest, apoptosis, inhibition of BCR-ABL1/STAT5 signaling and modulation of other survival pathways [21,22,43]. Accordingly, we have previously shown that quinone-containing compounds inhibit CML cell growth through cell cycle arrest [21,22]. Examples include the NPQ-based derivative CM363, which induces cell cycle arrest through augmented S phase [21], and the NPQ-coumarin hybrid NPQ-C6, which increases subG1 and reduces G0/G1 cell cycle phases [22]. In the present study, we demonstrate that JKST6 alters the CML cell cycle by augmenting subG1 and reducing G0/G1 phases in a time- and dose-dependent manner with higher potency than its precursor NPQ-C6 [22]. Importantly, these effects are associated with changes in the phosphorylation and/or expression of several proteins involved in cell cycle progression. Thus, JKST6 reduced retinoblastoma (RB) phosphorylation, which is necessary for cell cycle progression and is normally associated with cyclin

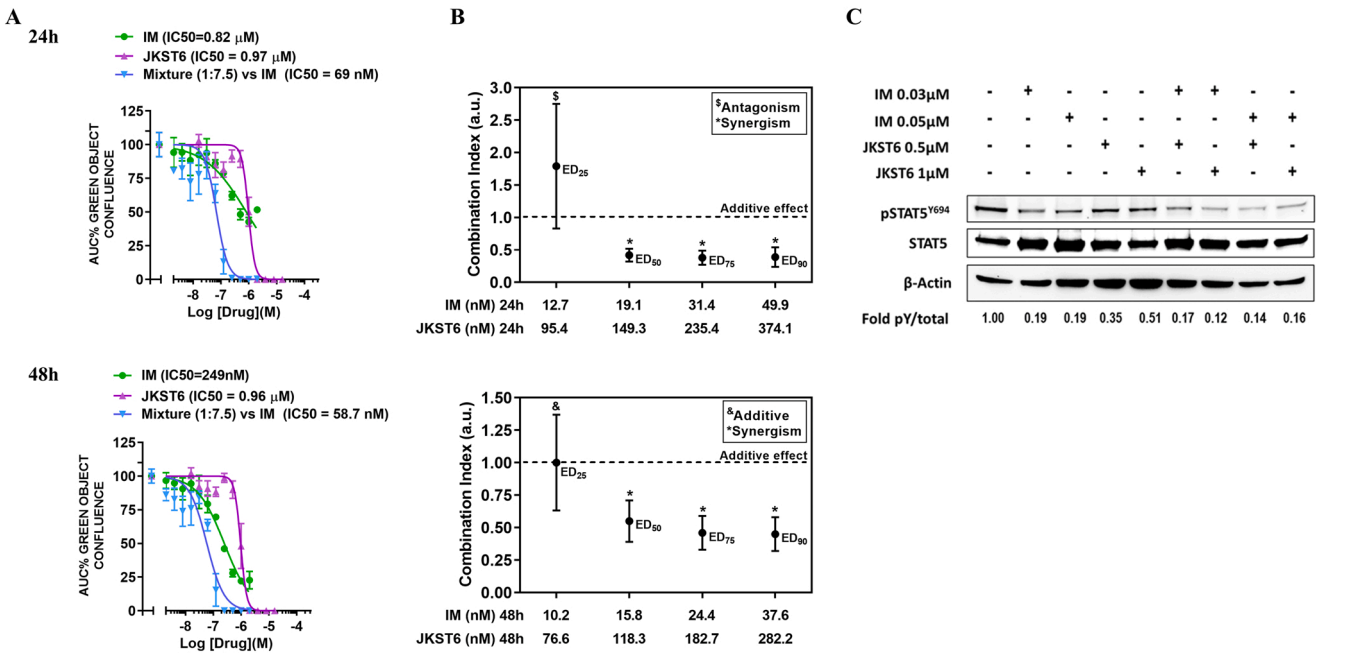


**Fig. 7. JKST6 and imatinib coadministration acts synergistically in cell proliferation and STAT5 phosphorylation inhibition. (A)** Representative image of cell proliferation measured in K562-GFP+ cells exposed to a constant ratio combination of different concentrations of JKST6 and imatinib (IM) (Mixture). Data are presented as the percentage of green confluence by IM concentration at 24 h (**upper panel**) and 48 h (**lower panel**). **(B)** Proliferation data analyzed by isobologram in K562-GFP+ cells treated with JKST6 (8 doses; from 0 to 5 μM), IM (8 doses; from 0 to 1 μM) or both in combination (constant ratio design (7.5 (JKST6):1 (IM)) for 24 and 48 h. The effect varied from 0 (no cell proliferation inhibition) to 1 (100% cell proliferation inhibition) using Calcusyn® software, as described in the Materials and Methods. Data are representative of four independent experiments with four replicates each. CI values (mean ± SEM) for ED25, ED50, ED75 and ED90 are symbolized as $ (antagonism), & (additive) or * (synergism). (C) Immunoblotting analysis of phosphorylated and total levels of STAT5 in whole cell lysates from K562 cultures treated with vehicle (0.05% DMSO), JKST6 (0.5 or 1 μM), IM (0.03 or 0.05 μM) or both drugs for 3 h. β-actin was used as a loading control. Images are representative of at least two independent experiments.

**Table 3**
Effects of JKST6 and IM on IM-sensitive or -resistant chronic myelogenous leukemia (CML) cells.

| Cell line | JKST6- IC50 values (μM; mean ±SEM) | IM- IC50 values (μM; mean ±SEM) |
|---|---|---|
| K562 | 0.66 ± 0.29 | 0.14 ± 0.05 |
| K562-R | 1.03 ± 0.13 | 3.86 ± 0.37 |
| AR230 | 1.52 ± 0.31 | 0.15 ± 0.02 |
| AR230-R | 1.57 ± 0.49 | 1.89 ± 0.55 |
| KmycBT315I | 1.79 ± 0.25 | 15.13 ± 1.72 |

Cells were treated with vehicle (0.05% DMSO), JKST6 (0.01–10 μM) or IM (0.03–20 μM) for 48 h. Then, cell viability was assessed by MTT assays as described in Material and Methods.

D/Cdk4 inhibition [44]. Downregulation of RB phosphorylation has also been related to c-ABL kinase inhibition, which in turn plays a role in S phase progression [45]. Moreover, complexes formed by cyclin E-CDK2, cyclin A-CDK2 and cyclin B-CDK1 regulate the G1/S transition, S phase progression, and G2/M transition, respectively [46]. Interestingly, JKST6 modulates these cyclins together with a significant increase in pCDK1$^{Y15}$. This phosphorylation leads to CDK1 inactivation, which is controlled by the Wee1 and Cdc25 balance [46]. NPQ-containing compounds have been previously identified as Cdc25 inhibitors [21,47], which block phosphatase activity and therefore CDK1 activation. Moreover, the phosphorylation of Wee1 at S$^{642}$ has been reported to be AKT-dependent and to cause Wee1 inactivation [48]. In fact, JKST6 transiently induces pWee1$^{S642}$, which coincides with CDK1 active/-inactive states. Similarly, JKST6 reduces mitotic histone 3 (H3) phosphorylation at Ser-10 (pH 3$^{S10}$), which has been reported to be required for proper execution of mitosis [49]. Furthermore, JKST6 induces the expression of p21 protein, a negative regulator of G1 and G2 progression, which has been related to the antiproliferative effects of other NPQs (e.g., shikonin and plumbagin) on leukemic cells [43,50]. In addition, JKST6 strongly stimulates phosphorylation of the downstream effectors of the ATM/ATR-dependent DNA damage checkpoint (pChk1$^{S296}$ and pChk2$^{T68}$) at short times after compound exposure, suggesting an early and potent induction of genotoxicity by the compound [51], which is a reported feature of NPQs and pyrones [52]. All these findings support the hypothesis that JKST6 prevents cell cycle progression by inducing cell arrest in the subG1 phase and triggering mitosis alterations, effects that might be caused, at least in part, by DNA damage.

Loss of apoptotic control allows cancer cells to survive longer; therefore, regulation of apoptosis constitutes a hotspot for any antitumoral drug. In this sense, JKST6 induces apoptosis in K562 cells, as assessed by increased Annexin V activity, apoptotic nuclei, activation of caspase-8, −9 and −3 and PARP cleavage. Previous studies have shown that NPQ derivatives and hybrids are able to induce apoptosis in CML cells through the induction of the intrinsic mitochondrial-dependent pathway [21,22,43], which involves the activation of caspases 9 and 3. However, the activation of caspase-8 (apoptosis extrinsic pathway) has also been implicated in NPQ-induced apoptosis in human leukemia cells [53]. Paradoxically, JKST6 upregulates the antiapoptotic protein Mcl-1, an effect that has also been reported in myeloid leukemia cells in response to certain chemotherapeutics [54]. Notably, JKST6 promotes an early increase in the double-strand DNA break marker γH2AX, further reinforcing the hypothesis that the compound triggers DNA damage related to the apoptotic process that cannot be repaired by CML cells.

Cell cycle arrest and activation of apoptosis induced by NPQ-based derivatives and hybrids in CML cells are generally associated with potent downregulation of BCR-ABL1/STAT5 signaling [21,22]. Accordingly, JKST6 leads to a rapid decrease in BCR-ABL1 phosphorylation (p$^{Y412}$ and p$^{Y177}$) in CML cells, which can be explained by a concomitant reduction in its total protein levels. These fast responses are

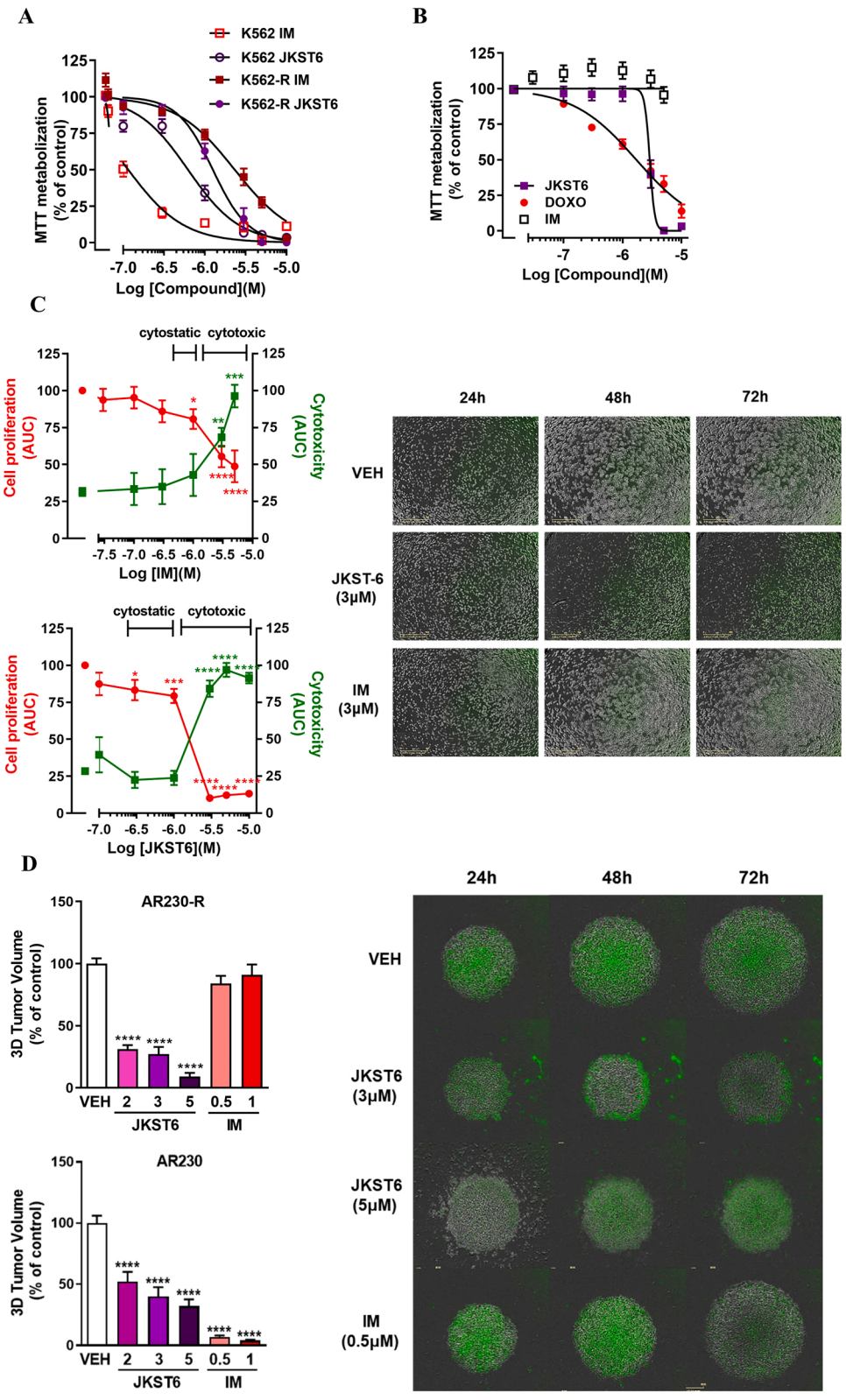


**Fig. 8. JKST6 reduces cell viability and growth and downregulates the BCR-ABL1/STAT5 signaling pathway in imatinib (IM)-resistant cells. (A)** Cell viability measured in IM-sensitive (K562) cells (□, ○) and IM-resistant (K562-R) cells (■, ●) incubated with vehicle (0.05% DMSO) or different concentrations of JKST6 (○,●) or IM (□, ■) for 48 h. **(B)** Cell viability measured in K562-R cultures exposed to vehicle or graded concentrations (0.01–10 μM) of JKST6 (●), DOXO (●) or IM (○) for 3 h, followed by wash-out steps as explained in the Materials and Methods. **(C)** Proliferation (●) and cytotoxicity (■) measured with the IncuCyte™ HD real-time analysis system in K562-R cells treated with vehicle, JKST6 (0.01–10 μM) or IM (0.01–5 μM) for 5 days. Data are plotted as the *area under the curve* (AUC) by JKST6 dose (**left panel**). Representative microphotographs of proliferating K562-R cells in the absence (vehicle (0.05% DMSO): VEH) or presence of JKST6 (3 μM) or IM (3 μM) for 24, 48 and 72 h (right panel). **(D)** 3D cultures of IM-sensitive AR230 and IM-resistant AR230-R cells treated with JKST6 (2, 3 and 5 μM), IM (0.5 and 1 μM) or VEH for 5 days. Spheroid growth and cytotoxicity were monitored using the IncuCyte real-time system, and tumor volume was calculated as the percentage of the control in AR230-R (**upper left panel**) and AR230 cells (**lower left panel**). Illustrative microphotographs of AR230-R tumor spheroids in the absence (VEH) or presence of compounds JKST6 (3 and 5 μM) or IM (0.5 μM) for 24, 48 or 72 h (right panel). Figures are representative of at least two independent experiments, each performed in triplicate. Statistical significance was assessed using one-way ANOVA with Bonferroni post hoc test. $^{*}P < 0.05$; $^{**}P < 0.01$; $^{***}P < 0.001$; $^{****}P < 0.0001$ versus VEH-treated cells.

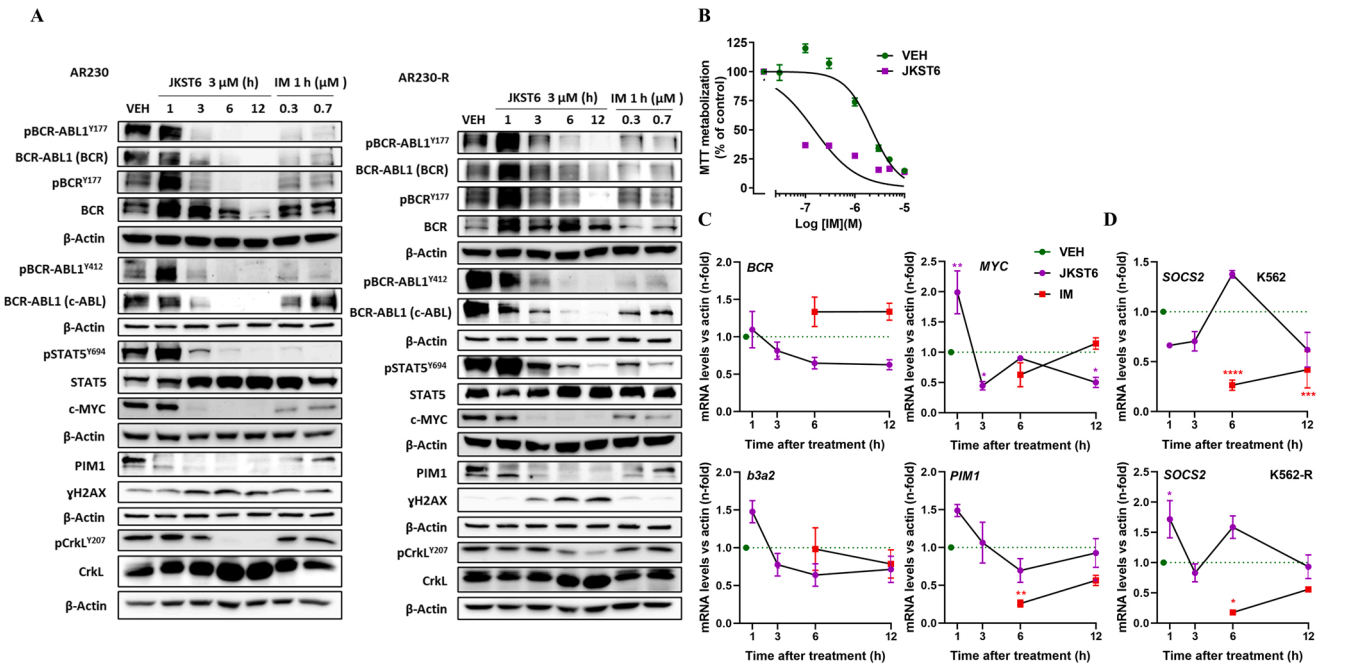


**Fig. 9. JKST6 blocks the BCR-ABL1/STAT5 signaling pathway and downstream target effectors in IM-resistant cells.(A)** Immunoblotting detection of phosphorylated and total levels of BCR-ABL1, BCR, STAT5, CrkL, c-MYC, and PIM1 and the presence of γH2AX in whole-cell extracts of AR230 **(left panel)** and AR230-R **(right panel)** cells treated with vehicle (VEH; 0.05% DMSO), JKST6 (3 μM) or imatinib (IM) (0.3 or 0.7 μM) for the indicated times. β-actin was used as a loading control. Figures are representative of two independent experiments. **(B)** Cell viability measured in AR230-R cells pretreated with VEH (●) or JKST6 (3 μM, ●) for 3 h prior to wash-out steps, followed by IM treatment (0.01–10 μM). Figures are representative of two independent experiments, each performed in triplicate. **(C)** mRNA expression analysis by qPCR of BCR-ABL1/STAT5 axis-target oncogenes (*BCR; b3a2; PIM1, c-MYC* and the housekeeper *GAPDH*) in IM-resistant (K562-R) cells. **(D)** *SOCS2* mRNA expression analyzed in K562 **(upper panel)** and K562-R cells **(lower panel)** treated with VEH (●), JKST6 (3 μM, ●) or IM (1 μM, ■) for the indicated times. Data are presented as the mean ± SEM of three independent experiments, each performed in duplicate. Statistical significance was assessed using one-way ANOVA with Bonferroni post hoc test. *$P < 0.05$; **$P < 0.01$; *** $P < 0.001$; ****$P < 0.0001$ versus VEH-treated cells.

often associated with posttranslational events, predominantly regulated by ubiquitin conjugation and proteasome activation [55]. In fact, a rapid decrease in BCR-ABL1 protein levels has been described for drugs that alter the ubiquitin cycle [14,56]. Accordingly, JKST6-induced downregulation of BCR-ABL1 protein was preceded by an increased level of polyubiquitinated proteins. Importantly, previous inhibition of the proteasome by MG132 [34] followed by JKST6 treatment partially prevented JKST6-induced BCR-ABL1 protein downregulation at 1 h after treatment and provoked an increased level of polyubiquitinated proteins. These findings suggest that proteasome activation might contribute, at least in part, to the effects of JKST6 on CML. Moreover, protein polyubiquitination and decay were followed by a reduction in *BCR-ABL1* mRNA levels, which supports the hypothesis that protein degradation precedes the inhibition of gene transcription. Although the exact posttranslational mechanism implicated in these effects deserves future research, compounds that cause ubiquitin cycle disturbances have been described as a successful approach to reduce BCR-ABL1 levels and subsequently activate cell death even in IM-resistant CML cells [14].

Interestingly, the rapid inhibition of BCR-ABL1 is effective downstream. In particular, the JKST6-induced inhibition of pSTAT5$^{Y694}$ predictably plays a key role in the antiproliferative effects of this compound due to its crucial roles in cell transformation, survival and growth in this neoplasm [4]. JKST6 also shows important functional effects inferred from the inhibition of pCrkL$^{Y207}$ and STAT5 target genes, such as PIM1 and c-MYC. These findings are particularly relevant, as c-MYC and BCR-ABL1 can upregulate each other; *MYC* participates in cell transformation, genomic instability and suppression of cell differentiation, thus favoring a poor response to IM and therefore a higher aggressiveness of disease [22,27]. Moreover, c-MYC inhibition caused by NPQ-based derivatives and hybrids has directly been linked with apoptosis induction in CML [21,22,57]. PIM1 is also upregulated by BCR-ABL1/STAT5 signaling and has roles in cell survival, transformation, and apoptosis protection against DNA damage [58]. Furthermore, PIM1 inhibition has been seen to play a central role in the anti-CML pharmacological actions of NPQ-based derivatives and hybrids [21,22]. Interestingly, we observed that JKST6 also had a regulatory role in STAT-mediated transcriptional activity, evidenced by the inhibition of IL3/JAK2/STAT5-dependent transcription. Taken together, these results support the hypothesis that JKST6 downregulates the BCR-ABL1/STAT5 signaling pathway as part of its anti-CML properties.

BCR-ABL1 exerts proleukemic actions by modulating additional signaling pathways, such as PI3K/AKT/mTOR and RAS/MAPK [4]. Notably, JKST6 inhibits the activation of the Src family of kinases, in contrast to IM, which is important due to the involvement of Src deregulated signaling in CML progression and TKI resistance [12]. Remarkably, JKST6 modulates MAPK signaling in CML cells, inducing transient activation of JNK, moderate inhibition of p38MAPK activation, and sustained phosphorylation of ERK1/2. Conversely, other NPQ-based derivatives and hybrids have been shown to downregulate ERK1/2 phosphorylation concomitantly with their antiproliferative actions in CML cells [21,22,43]. However, it has also been described that pERK1/2$^{T202/Y204}$ induction is related to activated apoptosis in human leukemia cells [59], which may explain the results observed with JKST6. Alternatively, JNK transient stimulation and pP38MAPK$^{T180/Y182}$ downregulation have already been reported to be associated with the antiproliferative effects of NPQ derivatives and hybrids in CML [21,22]. Interestingly, the BCR-ABL1/GBR-2 complex recruits and stimulates PI3K in CML cells, and subsequently, AKT and mTOR are activated and promote cell growth and survival [60]. mTOR signaling controls mRNA translation via its direct effector, the ribosomal protein S6 [60]. Furthermore, it has been reported that the constitutive activation of mTOR observed in several tumors can downregulate receptor tyrosine kinase signaling (e.g., IGF-IR) and, eventually, AKT activation as a negative feedback mechanism [61]. Interestingly, JKST6 potently and

rapidly inhibits S6 and increases pAKT$^{T308/S473}$, effects that suggest that the compound might inhibit mTOR. However, whether JKST6 exerts rapamycin-like effects in CML and the relevance of these potential properties on its molecular mechanism of action require further research.

TKI intolerance and IM resistance are current key challenges in CML therapy [8]. Therefore, one of the crucial aspects within the studied JKST6 properties has been its ability to potentiate the TKI effect and overcome IM resistance. JKST6 acts synergistically with IM, inhibiting cell proliferation and STAT5 activation in K562 cells, which is a promising finding because it opens an opportunity to reduce the effective dose of IM and, subsequently, the risk of long-term associated toxicity. In addition, JKST6 is highly effective in both AR230-R and K562-R cells, where IM resistance is mainly associated with increased BCR-ABL1 expression [36] or overexpression of Src family kinases [62], respectively. Similarly, JKST6 is highly effective on K562mycT315I cells, whose IM resistance is linked to a point mutation at the so-called gatekeeper residue of BCR-ABL1 [11]. Importantly, this mutation confers resistance to not only IM but also second-generation BCR-ABL1 inhibitors such as dasatinib and nilotinib [63]. JKST6 inhibition of the BCR-ABL1/STAT5 signaling pathway in AR230-R cells supports the hypothesis that the compound maintains its mechanistic modulation against the hyperactivation of the oncogenic pathway, suggesting an important utility of JKST6 in an already established IM-resistance context. The efficacy of JKST6 on CML-resistant cells was further corroborated by the inhibition of *MYC* and *PIM1* mRNA levels [4]. SOCS2, a ubiquitin ligase that negatively regulates the JAK-STAT pathway [64], has been described to be overexpressed in BCR-ABL1 + cells, and this expression could be downregulated by IM treatment. Moreover, refractory and relapse responses to IM are associated with enhanced SOCS2 expression [65]. Accordingly, our results showed higher basal *SOCS2* mRNA levels in IM-resistant cells than in IM-sensitive cells. Additionally, significant IM-induced downregulations of *SOCS2* expression were detected in both cell lines, contrasting with the described IM inability to modulate SOCS2 in resistant cells. This difference could be a result of the different mechanism of resistance present in K562-R cells, which is related to Lyn overexpression. Conversely, JKST6 stimulated *SOCS2* expression after 6 h of treatment in both K562-R and K562 cells, which might contribute to the negative regulation of BCR-ABL1/STAT5 signaling in these cells. In fact, SOCS2 overexpression may play a role in the ubiquitination of BCR-ABL1 induced by JKST6 treatment since the SOCS family participates in target protein degradation [66]. Interestingly, JKST6 is able to circumvent IM resistance in CML cells overexpressing BCR-ABL1, probably largely motivated by a reduction in oncokinase levels, which seems effective in restoring sensitivity to TKI treatment.

## 5. Conclusions

In summary, JKST6 possesses a combination of interesting properties that make it into a promising compound to further study in order to overcome the main CML therapy limitations. First, JKST6 efficiently reduces BCR-ABL1, preventing not only its constitutive activation but also its function as a “scaffold protein” that in turn modulates alternative survival pathways. Second, this effective feature of JKST6 activity is maintained in cells that are resistant to IM by BCR-ABL1-dependent or BCR-ABL1-independent mechanisms. Third and clinically relevant, JKST6 potentiates IM-induced antitumoral effects, suggesting that it could be considered in combinatorial therapy with TKIs in CML.

## Funding

This research has been funded by Spanish Ministry of Economy and Competitiveness - MINECO - (SAF 2015–65113-C2–1-R and RTI2018–094356-B-C21 to AEB, SAF2015–65113-C2–2 to LFP, SAF2017–88026-R to JL) with the co-funding of European Regional Development Fund (EU-ERDF), Canary Islands Government (CEI2018–23/ACIISI to BG, CEI2019–08/ACIISI to BG and LFP, ProID2021010037 to AEB, LFP and BG) and "Juan de la Cierva Incorporacion" Grant Program from the Ministry of Science, Innovation and Universities (IJC2018-035193-I to CR). This project has been also supported by Alfredo Martin-Reyes Foundation (Arehucas)-Canary Islands Foundation for Cancer Research (FICIC). HAT is recipient of a predoctoral program grant from ULPGC (2016). JCM was funded by the Instituto de Salud Carlos III through a Miguel Servet program (CPII17/00015).

## CRediT authorship contribution statement

***Haidée Aranda-Tavío***: Conceptualization, Validation, Formal analysis, Investigation, Data curation, Writing - original draft, Writing - review & editing, Visualization, Project administration. ***Carlota Recio***: Conceptualization, Validation, Formal analysis, Investigation, Data curation, Writing - Original Draft, Writing - review & editing, Visualization, Supervision, Project administration, Funding acquisition. ***Pedro Martín-Acosta***: Conceptualization, Validation, Formal analysis, Investigation, Data curation, Writing - review & editing. ***Miguel Guerra-Rodríguez***: Validation, Formal analysis, Investigation, Data curation, Visualization, Project administration. ***Yeray Brito-Casillas***: Conceptualization, Validation, Formal analysis, Investigation, Writing - review & editing, Resources, Supervision. ***Rosa Blanco***: Validation, Formal analysis, Investigation. ***Vanessa Junco***: Validation, Formal analysis, Investigation, Writing - review & editing. ***Javier León***: Conceptualization, Validation, Formal analysis, Investigation, Resources, Data Curation, Writing - review & editing. ***Juan Carlos Montero***: Conceptualization, Validation, Formal analysis, Investigation, Writing - review & editing. ***Lucía Gandullo-Sánchez***: Conceptualization, Validation, Formal analysis, Investigation, Writing - review & editing. ***Grant McNaughton-Smith***: Conceptualization, Validation, Formal analysis, Investigation, Resources, Writing - Review & Editing. ***Juan M. Zapata***: Resources. ***Atanasio Pandiella***: Conceptualization, Investigation, Resources. ***Ángel Amesty***: Conceptualization, Validation, Formal analysis, Investigation, Data Curation, Writing - review & editing. ***Ana Estévez-Braun***: Conceptualization, Validation, Formal analysis, Investigation, Resources, Data Curation, Writing - review & editing, Supervision, Project administration, Funding acquisition. ***Leandro Fernández-Pérez***: Conceptualization, Formal analysis, Investigation, Resources, Data Curation, Writing - original draft, Writing - review & editing, Supervision, Project administration, Funding acquisition. ***Borja Guerra***: Conceptualization, Formal analysis, Investigation, Resources, Data Curation, Writing - original draft, Writing - review & editing, Visualization, Supervision, Project administration, Funding acquisition.

## Conflict of interest statement

The authors declare that there are no conflicts of interest in this work.

## Appendix A. Supporting information

Supplementary data associated with this article can be found in the online version at doi:10.1016/j.biopha.2021.112330.

## References

[1] R. Ren, Mechanisms of BCR-ABL in the pathogenesis of chronic myelogenous leukaemia, Nat. Rev. Cancer 5 (2005) 172–183, https://doi.org/10.1038/nrc1567.
[2] B. Johansson, T. Fioretos, F. Mitelman, Cytogenetic and molecular genetic evolution of chronic myeloid leukemia, Acta Haematol. 107 (2002) 76–94, https://doi.org/10.1159/000046636.
[3] R. Kurzrock, J.U. Gutterman, M. Talpaz, The molecular genetics of philadelphia chromosome–positive leukemias, N. Engl. J. Med. 319 (1988) 990–998, https://doi.org/10.1056/NEJM198810133191506.

[4] C. Recio, B. Guerra, M. Guerra-Rodríguez, H. Aranda-Tavío, P. Martín-Rodríguez, M. de Mirecki-Garrido, Y. Brito-Casillas, J.M. García-Castellano, A. Estévez-Braun, L. Fernández-Pérez, Signal transducer and activator of transcription (STAT)-5: an opportunity for drug development in oncohematology, Oncogene 38 (2019) 4657–4668, https://doi.org/10.1038/S41388-019-0752-3.

[5] W. Warsch, E. Grundschober, V. Sexl, Adding a new facet to STAT5 in CML multitasking for leukemic cells, Cell Cycle 12 (2013) 1813–1814, https://doi.org/10.4161/cc.25116.

[6] D. Vetrie, G.V. Helgason, M. Copland, The leukaemia stem cell: similarities, differences and clinical prospects in CML and AML, Nat. Rev. Cancer 20 (2020) 158–173, https://doi.org/10.1038/s41568-019-0230-9.

[7] A. Sinclair, A.L. Latif, T.L. Holyoake, Targeting survival pathways in chronic myeloid leukaemia stem cells, Br. J. Pharm. 169 (2013) 1693–1707, https://doi.org/10.1111/bph.12183.

[8] R. Hehlmann, Chronic myeloid leukemia in 2020, HemaSphere 4 (2020), e468, https://doi.org/10.1097/hs9.0000000000000468.

[9] A. Hochhaus, M. Baccarani, R.T. Silver, C. Schiffer, J.F. Apperley, F. Cervantes, R. E. Clark, J.E. Cortes, M.W. Deininger, F. Guilhot, H. Hjorth-Hansen, T.P. Hughes, J. J.W.M. Janssen, H.M. Kantarjian, D.W. Kim, R.A. Larson, J.H. Lipton, F.X. Mahon, J. Mayer, F. Nicolini, D. Niederwieser, F. Pane, J.P. Radich, D. Rea, J. Richter, G. Rosti, P. Rousselot, G. Saglio, S. Saußele, S. Soverini, J.L. Steegmann, A. Turkina, A. Zaritskey, R. Hehlmann, European LeukemiaNet 2020 recommendations for treating chronic myeloid leukemia, Leukemia 34 (2020) 966–984, https://doi.org/10.1038/s41375-020-0776-2.

[10] S.B. Dusetzina, A.N. Winn, G.A. Abel, H.A. Huskamp, N.L. Keating, Cost sharing and adherence to tyrosine kinase inhibitors for patients with chronic myeloid leukemia, J. Clin. Oncol. 32 (2014) 306–311, https://doi.org/10.1200/JCO.2013.52.9123.

[11] J. Cortes, F. Lang, Third-line therapy for chronic myeloid leukemia: current status and future directions, J. Hematol. Oncol. 14 (2021) 1–18, https://doi.org/10.1186/s13045-021-01055-9.

[12] A. Quintás-Cardama, H.M. Kantarjian, J.E. Cortes, Mechanisms of primary and secondary resistance to imatinib in chronic myeloid leukemia, Cancer Control 16 (2009) 122–131, https://doi.org/10.1177/107327480901600204.

[13] S. Grosso, A. Puissant, M. Dufies, P. Colosetti, A. Jacquel, K. Lebrigand, P. Barbry, M. Deckert, J.P. Cassuto, B. Mari, P. Auberger, Gene expression profiling of imatinib and PD166326-resistant CML cell lines identifies Fyn as a gene associated withresistance to BCR-ABL inhibitors, Mol. Cancer Ther. 8 (2009) 1924–1933, https://doi.org/10.1158/1535-7163.MCT-09-0168.

[14] H. Sun, V. Kapuria, L.F. Peterson, D. Fang, W.G. Bornmann, G. Bartholomeusz, M. Talpaz, N.J. Donato, Bcr-Abl ubiquitination and Usp9x inhibition block kinase signaling and promote CML cell apoptosis, Blood 117 (2011) 3151–3162, https://doi.org/10.1182/blood-2010-03-276477.

[15] M. Brehme, O. Hantschel, J. Colinge, I. Kaupe, M. Planyavsky, T. Köcher, K. Mechtler, K.L. Bennett, G. Superti-Furga, Charting the molecular network of the drug target Bcr-Abl, Proc. Natl. Acad. Sci. U. S. A. 106 (2009) 7414–7419. https://doi.org/10.1073/pnas.0900653106.

[16] A. Ocaña, A. Pandiella, Proteolysis targeting chimeras (PROTACs) in cancer therapy, J. Exp. Clin. Cancer Res. 39 (2020) 1–9, https://doi.org/10.1186/s13046-020-01672-1.

[17] E. Vuelta, I. García-Tuñón, P. Hernández-Carabias, L. Méndez, M. Sánchez-Martín, Future approaches for treating chronic myeloid leukemia: crispr therapy, in: Biology, 10, Basel,, 2021, pp. 1–16, https://doi.org/10.3390/biology10020118.

[18] F. Loscocco, G. Visani, S. Galimberti, A. Curti, A. Isidori, BCR-ABL independent mechanisms of resistance in chronic myeloid leukemia, Front. Oncol. 9 (2019) 1–11, https://doi.org/10.3389/fonc.2019.00939.

[19] H.-Y. Qiu, P.-F. Wang, H.-Y. Lin, C.-Y. Tang, H.-L. Zhu, Y.-H. Yang, Naphthoquinones: a continuing source for discovery of therapeutic antineoplastic agents, Chem. Biol. Drug Des. 91 (2018) 681–690, https://doi.org/10.1111/cbdd.13141.

[20] Z. Yin, J. Zhang, L. Chen, Q. Guo, B. Yang, W. Zhang, W. Kang, Anticancer effects and mechanisms of action of plumbagin: review of research advances, Biomed. Res. Int (2020)) (2020), https://doi.org/10.1155/2020/6940953.

[21] B. Guerra, P. Martin-Rodriguez, J.C. Diaz-Chico, G. McNaughton-Smith, S. Jimenez-Alonso, I. Hueso-Falcon, J.C.C. Montero, R. Blanco, J. Leon, G. Rodriguez-Gonzalez, A. Estevez-Braun, A. Pandiella, B.N. Diaz-Chico, L. Fernandez-Perez, CM363, a novel naphthoquinone derivative which acts as multikinase modulator and overcomes imatinib resistance in chronic myelogenous leukemia, Oncotarget 8 (2017) 29679–29698, https://doi.org/10.18632/oncotarget.11425 11425 [pii].

[22] P. Martín-Rodríguez, B. Guerra, I. Hueso-Falcón, H. Aranda-Tavío, J. Díaz-Chico, J. Quintana, F. Estévez, B. Díaz-Chico, A. Amesty, A. Estévez-Braun, L. Fernández-Pérez, A novel naphthoquinone-coumarin hybrid that inhibits BCR-ABL1-STAT5 oncogenic pathway and reduces survival in imatinib-resistant chronic myelogenous leukemia cells, Front. Pharmacol. 9 (2019), https://doi.org/10.3389/fphar.2018.01546.

[23] I.J.S. Fairlamb, L.R. Marrison, J.M. Dickinson, F.J. Lu, J.P. Schmidt, 2-Pyrones possessing antimicrobial and cytotoxic activities, Bioorganic Med. Chem. 12 (2004) 4285–4299, https://doi.org/10.1016/j.bmc.2004.01.051.

[24] Y. Wang, Z. Zhong, F. Zhao, J. Zheng, X. Zheng, K. Zhang, H. Huang, Two new pyrone derivatives from the mangrove-derived endophytic fungus Aspergillus sydowii #2B, Nat. Prod. Res. 0 (2021) 1–7, https://doi.org/10.1080/14786419.2021.1892673.

[25] R.M. Yang, X.L. Zhang, L. Wang, J.P. Huang, J. Yang, Y.J. Yan, J.Y. Luo, X.T. Wang, S.X. Huang, α-Pyrone derivatives from a Streptomyces strain resensitize tamoxifen resistance in breast cancer cells, Nat. Prod. Bioprospect 7 (2017) 329–334, https://doi.org/10.1007/s13659-017-0136-8.

[26] J.C. Estrada, Y. Torres, A. Benguría, A. Dopazo, E. Roche, L. Carrera-Quintanar, R. A. Pérez, J.A. Enríquez, R. Torres, J.C. Ramírez, E. Samper, A. Bernad, Human mesenchymal stem cell-replicative senescence and oxidative stress are closely linked to aneuploidy, Cell Death Dis. 4 (2013), https://doi.org/10.1038/cddis.2013.211.

[27] M. Albajar, M.T. Gómez-Casares, J. Llorca, I. Mauleon, J.P. Vaqué, J.C. Acosta, A. Bermúdez, N. Donato, M.D. Delgado, J. León, MYC in chronic myeloid leukemia: Induction of aberrant DNA synthesis and association with poor response to imatinib, Mol. Cancer Res. 9 (2011) 564–576, https://doi.org/10.1158/1541-7786.MCR-10-0356.

[28] T. Mosmann, Rapid colorimetric assay for cellular growth and survival: application to proliferation and cytotoxicity assays, J. Immunol. Methods 65 (1983) 55–63, https://doi.org/10.1016/0022-1759(83)90303-4.

[29] M. Vinci, S. Gowan, F. Boxall, L. Patterson, M. Zimmermann, W. Court, C. Lomas, M. Mendiola, D. Hardisson, S.A. Eccles, Advances in establishment and analysis of three-dimensional tumor spheroid-based functional assays for target validation and drug evaluation, BMC Biol. 10 (2012) 29, https://doi.org/10.1186/1741-7007-10-29.

[30] J. Ye, G. Coulouris, I. Zaretskaya, I. Cutcutache, S. Rozen, T.L. Madden, Primer-BLAST: a tool to design target-specific primers for polymerase chain reaction, BMC Bioinforma. 13 (2012) 134, https://doi.org/10.1186/1471-2105-13-134.

[31] T.D. Schmittgen, K.J. Livak, Analyzing real-time PCR data by the comparative CT method, Nat. Protoc. 3 (2008) 1101–1108, https://doi.org/10.1038/nprot.2008.73.

[32] T.C. Chou, Drug combination studies and their synergy quantification using the chou-talalay method, Cancer Res 70 (2010) 440–446, https://doi.org/10.1158/0008-5472.CAN-09-1947.

[33] S. Irwin, Irwin 1968 (1).pdf, Psychopharmacologia 13 (1968) 222–257.

[34] A.F. Kisselev, A.L. Goldberg, Proteasome inhibitors: from research tools to drug candidates, Chem. Biol. 8 (2001) 739–758, https://doi.org/10.1016/S1074-5521(01)00056-4.

[35] R. De Jong, J. Ten Hoeve, N. Heisterkamp, J. Groffen, Tyrosine 207 in CRKL is the BCR/ABL phosphorylation site, Oncogene 14 (1997) 507–513, https://doi.org/10.1038/sj.onc.1200885.

[36] F.X. Mahon, M.W.N. Deininger, B. Schultheis, J. Chabrol, J. Reiffers, J. M. Goldman, J.V. Melo, Selection and characterization of BCR-ABL positive cell lines with differential sensitivity to the tyrosine kinase inhibitor STI571: diverse mechanisms of resistance, Blood 96 (2000) 1070–1079, https://doi.org/10.1182/blood.v96.3.1070.015k17_1070_1079.

[37] C. Zheng, L. Li, M. Haak, B. Brors, O. Frank, M. Giehl, A. Fabarius, M. Schatz, A. Weisser, C. Lorentz, N. Gretz, R. Hehlmann, A. Hochhaus, W. Seifarth, Gene expression profiling of CD34+ cells identifies a molecular signature of chronic myeloid leukemia blast crisis, Leukemia 20 (2006) 1028–1034, https://doi.org/10.1038/sj.leu.2404227.

[38] R.A. Copeland, D.L. Pompliano, T.D. Meek, Drug-target residence time and its implications for lead optimization, Nat. Rev. Drug Discov. 5 (2006) 730–739, https://doi.org/10.1038/nrd2082.

[39] R. Lonsdale, R.A. Ward, Structure-based design of targeted covalent inhibitors, Chem. Soc. Rev. 47 (2018) 3816–3830, https://doi.org/10.1039/c7cs00220c.

[40] G.P. McGlacken, I.J.S. Fairlamb, 2-pyrone natural products and mimetics: Isolation, characterisation and biological activity, Nat. Prod. Rep. 22 (2005) 369–385, https://doi.org/10.1039/b416651p.

[41] S. Sant, P.A. Johnston, The production of 3D tumor spheroids for cancer drug discovery, Drug Discov. Today Technol. 23 (2017) 27–36, https://doi.org/10.1016/j.ddtec.2017.03.002.

[42] S. Zemenides, J. Dos Santos, L. Enfield, A. Mantalaris, N. Panoskaltsis, Metabolism of acute myeloid leukemia cell lines alters with passage in 2D culture and remains stable in 3D, 2787–2787, Blood 132 (2018), https://doi.org/10.1182/blood-2018-99-118648.

[43] C. Guo, J. He, X. Song, L. Tan, M. Wang, P. Jiang, Y. Li, Z. Cao, C. Peng, Pharmacological properties and derivatives of shikonin—a review in recent years, Pharmacol. Res. 149 (2019), https://doi.org/10.1016/j.phrs.2019.104463.

[44] R.A. Weinberg, The retinoblastoma protein and cell cycle control, Cell 81 (1995) 323–330, https://doi.org/10.1016/0092-8674(95)90385-2.

[45] P.J. Welch, J.Y.J. Wang, A C-terminal protein-binding domain in the retinoblastoma protein regulates nuclear c-Abl tyrosine kinase in the cell cycle, Natl. Libr. Med. 75 (4) (1993) 779–790.

[46] J.H. Lee, J.Y. Sung, E.K. Choi, H.-K. Yoon, B.R. Kang, E.K. Hong, B.-K. Park, Y.-N. Kim, S.B. Rho, K. Yoon, C/EBPβ Is a transcriptional regulator of Wee1 at the G2/M phase of the cell cycle, Cells 8 (2019) 145, https://doi.org/10.3390/cells8020145.

[47] A.K. Brenner, H. Reikvam, A. Lavecchia, Ø. Bruserud, Therapeutic targeting the cell division cycle 25 (CDC25) phosphatases in human acute myeloid Leukemia - the possibility to target several kinases through inhibition of the various CDC25 isoforms, Molecules 19 (2014) 18414–18447, https://doi.org/10.3390/molecules191118414.

[48] K. Katayama, N. Fujita, T. Tsuruo, Akt/protein kinase B-dependent phosphorylation and inactivation of WEE1Hu promote cell cycle progression at G2/M transition, Mol. Cell. Biol. 25 (2005) 5725–5737, https://doi.org/10.1128/mcb.25.13.5725-5737.2005.

[49] M.J. Hendzel, Y. Wei, M.A. Mancini, A. Van Hooser, T. Ranalli, B.R. Brinkley, D. P. Bazett-Jones, C.D. Allis, Mitosis-specific phosphorylation of histone H3 initiates primarily within pericentromeric heterochromatin during G2 and spreads in an

ordered fashion coincident with mitotic chromosome condensation, Chromosom 106 (6) (1997) 348–360, https://doi.org/10.1007/S004120050256.
[50] K.H. Xu, D.P. Lu, Plumbagin induces ROS-mediated apoptosis in human promyelocytic leukemia cells in vivo, Leuk. Res. 34 (2010) 658–665, https://doi.org/10.1016/j.leukres.2009.08.017.
[51] H. Zhao, H. Piwnica-Worms, ATR-mediated checkpoint pathways regulate phosphorylation and activation of human Chk1, Mol. Cell. Biol. 21 (2001) 4129–4139, https://doi.org/10.1128/mcb.21.13.4129-4139.2001.
[52] S.W. Newell, E.M. Perchellet, J.B. Ladesich, J.A. Freeman, Y. Chen, L. Liu, D. H. Hua, S.L. Kraft, R.J. Basaraba, J.P. Perchellet, Tricyclic pyrone analogs: a new class of microtubule-disrupting anticancer drugs effective against murine leukemia cells in vitro, Int. J. Oncol. 12 (1998) 433–442, https://doi.org/10.3892/ijo.12.2.433.
[53] X. Kong, J. Luo, T. Xu, Y. Zhou, Z. Pan, Y. Xie, L. Zhao, Y. Lu, X. Han, Z. Li, L. Liu, Plumbagin enhances TRAIL-induced apoptosis of human leukemic Kasumi-1 cells through upregulation of TRAIL death receptor expression, activation of caspase-8 and inhibition of cFLIP, Oncol. Rep. 37 (2017) 3423–3432, https://doi.org/10.3892/or.2017.5627.
[54] J.A. Vrana, E.S. Cleaveland, A. Eastman, R.W. Craig, Inducer-and cell type-specific regulation of antiapoptotic MCL1 in myeloid leukemia and multiple myeloma cells exposed to differentiation-inducing or microtubule-disrupting agents, Apoptosis 11 (2006) 1275–1288, https://doi.org/10.1007/s10495-006-7787-y.
[55] P. Grumati, I. Dikic, Ubiquitin signaling and autophagy, J. Biol. Chem. 293 (2018) 5404–5413, https://doi.org/10.1074/jbc.TM117.000117.
[56] G.A. Bartholomeusz, M. Talpaz, V. Kapuria, Y.K. Ling, S. Wang, Z. Estrov, W. Priebe, J. Wu, N.J. Donato, Activation of a novel Bcr/Abl destruction pathway by WP1130 induces apoptosis of chronic myelogenous leukemia cells, Blood 109 (2007) 3470–3478, https://doi.org/10.1182/blood-2006-02-005579.
[57] Z.L. Shan, L. Zhong, C.L. Xiao, L.G. Gan, T. Xu, H. Song, R. Yang, L. Li, B.Z. Liu, Shikonin suppresses proliferation and induces apoptosis in human leukemia NB4 cells through modulation of MAPKs and c-Myc, Mol. Med. Rep. 16 (2017) 3055–3060, https://doi.org/10.3892/mmr.2017.6965.
[58] K.J. Peltola, K. Paukku, T.L.T. Aho, M. Ruuska, O. Silvennoinen, P. Ivi, J. Koskinen, Pim-1 kinase inhibits STAT5-dependent transcription via its interactions with SOCS1 and SOCS3, Blood 103 (10) (2004), https://doi.org/10.1182/blood.
[59] E. Saavedra, H. Del Rosario, I. Brouard, J. Hernández-Garcés, C. García, J. Quintana, F. Estévez, The synthetic flavanone 6-methoxy-2-(naphthalen-1-yl) chroman-4-one induces apoptosis and activation of the MAPK pathway in human U-937 leukaemia cells, Bioorg. Chem. 94 (2020), 103450, https://doi.org/10.1016/J.BIOORG.2019.103450.
[60] W.C. Juan, S.T. Ong, The role of protein phosphorylation in therapy resistance and disease progression in chronic myelogenous leukemia, in: Prog. Mol. Biol. Transl. Sci., Elsevier B.V, 2012, pp. 107–142, https://doi.org/10.1016/B978-0-12-396456-4.00007-9.
[61] K.E. O'Reilly, F. Rojo, Q.B. She, D. Solit, G.B. Mills, D. Smith, H. Lane, F. Hofmann, D.J. Hicklin, D.L. Ludwig, J. Baselga, N. Rosen, mTOR inhibition induces upstream receptor tyrosine kinase signaling and activates Akt, Cancer Res 66 (2006) 1500–1508, https://doi.org/10.1158/0008-5472.CAN-05-2925.
[62] N.J. Donato, J.Y. Wu, J. Stapley, G. Gallick, H. Lin, R. Arlinghaus, M. Talpaz, BCR-ABL independence and LYN kinase overexpression in chronic myelogenous leukemia cells selected for resistance to STI571, Blood 101 (2003) 690–698, https://doi.org/10.1182/blood.V101.2.690.
[63] T. O'Hare, W.C. Shakespeare, X. Zhu, C.A. Eide, V.M. Rivera, F. Wang, L.T. Adrian, T. Zhou, W.-S. Huang, Q. Xu, C.A. Metcalf, J.W. Tyner, M.M. Loriaux, A.S. Corbin, S. Wardwell, Y. Ning, J.A. Keats, Y. Wang, R. Sundaramoorthi, M. Thomas, D. Zhou, J. Snodgrass, L. Commodore, T.K. Sawyer, D.C. Dalgarno, M.W. N. Deininger, B.J. Druker, T. Clackson, AP24534, a pan-BCR-ABL inhibitor for chronic myeloid leukemia, potently inhibits the T315I mutant and overcomes mutation-based resistance, Cancer Cell 16 (2009) 401–412, https://doi.org/10.1016/j.ccr.2009.09.028.
[64] A.N. Bullock, J.É. Debreczeni, A.M. Edwards, M. Sundström, S. Knapp, Crystal structure of the SOCS2–elongin C–elongin B complex defines a prototypical SOCS box ubiquitin ligase, Proc. Natl. Acad. Scii U. S. A. 103 (2006) 7637–7642, https://doi.org/10.1073/PNAS.0601638103.
[65] B. Schultheis, M. Carapeti-Marootian, A. Hochhaus, A. Weier, J.M. Goldman, J. V. Melo, Overexpression of SOCS-2 in advanced stages of chronicmyeloid leukemia: possible inadequacy of a negative feedback mechanism, Blood 99 (5) (2002). ⟨http://ashpublications.org/blood/article-pdf/99/5/1766/1681182/h8050201766.pdf⟩.
[66] J. Piessevaux, D. Lavens, F. Peelman, J. Tavernier, The many faces of the SOCS box, Cytokine Growth Factor Rev. 19 (2008) 371–381, https://doi.org/10.1016/J.CYTOGFR.2008.08.006.